

CHANS-SD-YRB V1.0: A System Dynamics model of the coupled human-natural systems for the Yellow River Basin

Shan Sang^{1,2}, Yan Li^{1,2*}, Shuang Zong^{1,2}, Lu Yu^{1,2}, Shuai Wang^{1,2}, Yanxu Liu^{1,2},
Xutong Wu^{1,2}, Shuang Song^{1,2}, Wenwu Zhao^{1,2}, Xuhui Wang³, Bojie Fu⁴

¹State Key Laboratory of Earth Surface Processes and Hazards Risk Governance (ESPHR), Beijing
Normal University, Beijing, China

²Institute of Land Surface System and Sustainable Development, Faculty of Geographical Science,
Beijing Normal University, Beijing, China

³Institute of Carbon Neutrality, Laboratory for Earth Surface Processes, College of Urban and
Environmental Sciences, Peking University, Beijing 100871, China

⁴State Key Laboratory of Regional and Urban Ecology, Research Center for Eco-Environmental
Sciences, Chinese Academy of Sciences, Beijing 100085, China

Corresponding Author:

Yan Li, Ph.D.

Institute of Land Surface System and Sustainable Development, Faculty of Geographical Science,
Beijing Normal University, Beijing, 100875, China

Email: yanli.geo@gmail.com

Abstract: Modeling the coupled human–natural systems (CHANS) is vital for understanding human–natural interactions and achieving regional sustainability, offering a powerful tool to alleviating human–water conflicts, ensuring food security, thereby supporting the region’s pathway toward sustainable development. However, the scarcity of regional-scale CHANS models constrains progress in practical applications for regional sustainability. The Yellow River basin (YRB) is an ideal region

27 for modeling regional CHANS due to its closely coupled human and natural systems,
28 which are stressed by water and ecosystem fragility. Here, we developed the CHANS-
29 SD-YRB model using the System Dynamics approach, integrating 10 sectors essential
30 for modeling human-water interactions of the basin, including five human sectors
31 (Population, Economy, Energy, Food, and Water Demand) and five natural sectors
32 (Water Supply, Sediment, Land, Carbon, and Climate). The model can simulate
33 evolution and feedbacks of the YRB CHANS annually at provincial and sub-basin
34 scales, while conserving hydrological connectivity between sub-basins. The model can
35 accurately reproduce historical CHANS dynamics, achieving strong quantitative
36 agreement with historical data ($R > 0.95$ for human sectors and $R > 0.7$ for natural
37 sectors), which supports its applicability for scenario analyses and future projections.
38 We applied the model to explore human–natural system dynamics under a future
39 baseline scenario, assuming the continuation of existing policies and climate projection
40 under middle of the road scenario (SSP–RCP 2-4.5). The future projections (2021-2100)
41 indicate that achieving sustainable development in the YRB will remain challenging,
42 though economic growth and food security are expected to improve. Emerging issues,
43 such as ecological–human water trade-offs, labor shortages, reduced sediment load, and
44 limited carbon absorption capacity, may hinder regional long-term sustainability.

45 **Keywords:** coupled human-natural systems, regional modeling, system dynamics,
46 the Yellow River Basin

47 **1 Introduction**

48 Coupled human and natural systems (CHANS) emphasize the reciprocal feedback
49 and co-evolution between human and natural systems, offering an integrated framework
50 for diagnosing complex problems and guiding sustainable development (Fu and Li,
51 2016). ~~While global-scale CHANS research has deepened our knowledge of dynamic~~
52 ~~feedbacks among Earth's spheres and system evolution under climate change,~~
53 ~~sustainability challenges often manifest at regional scales, where social and ecological~~
54 ~~dynamics are more intricately intertwined (Liu et al., 2007). Compared to global~~

55 ~~CHANS, regional CHANS are open systems that continuously exchange energy and~~
56 ~~materials with other regions and the global system, e.g., water resources and electricity~~
57 ~~transfers and trade, resulting in pericoupling and telecoupling of different systems~~
58 ~~(Liu, 2017). Besides, regional CHANS are shaped by more immediate and complex~~
59 ~~human influences and stressors, such as urban expansion, ecological protection (Xu et~~
60 ~~al., 2017; Yang et al., 2022), and water resource regulation policies (diversion and~~
61 ~~allocation) (Song et al., 2024), which alter regional CHANS dynamics. Moreover, due~~
62 ~~to their diverse ecological and socioeconomic resilience, regional CHANS exhibit~~
63 ~~heterogeneous responses to external weather events and climate change, as evidenced~~
64 ~~by differing responses in crop yield and economic production to extreme heat and~~
65 ~~warming.~~ By capturing dynamic interactions of interconnected components, CHANS
66 theories and models enable more effective policies and interventions that align
67 ecological integrity with socioeconomic progress (Motesharrei et al., 2016; Verburg et
68 al., 2016). ~~As such, advancing CHANS research is essential for informing adaptive~~
69 ~~strategies in the face of regional growing environmental and societal pressures.~~

70 ~~Modeling of CHANS is a frontier area of geographical science and has become a~~
71 ~~key approach in resources, environment, and climate research. CHANS models serve~~
72 ~~as essential tools for analyzing the complex dynamics of human–natural interactions~~
73 ~~and guiding pathways toward sustainability.~~ Numerous modeling-integrated modelling
74 approaches have been developed to simulate human–natural interactions at the global
75 scale, including These include system dynamics (SD)-based integrated assessment
76 models (e.g., IAMs), such as ANEMI (Breach and Simonovic, 2021), FeliX (Rydzak et
77 al., 2013; Ye et al., 2024), and FRIDA (Rajah et al., 2025)), ~~integrated assessment~~
78 ~~models (IAMs), process-based and optimization-based IAMs (Vaidyanathan, 2021),~~
79 and Earth system models with synchronously coupled human components, such as
80 E3SM-GCAM (Di Vittorio et al., 2025) and integrated Earth system ~~model~~
81 ~~(iESM models (iESMs) (Jain et al., 2022) and synchronously coupled human~~
82 ~~component in the earth system model (E3SM-GCAM)).~~ These models effectively

83 characterize human–natural interactions at the global scale, and have been applied to
84 assess the impacts of climate change on human society (e.g., agriculture (Monier et al.,
85 2018), economic damage (Wang et al., 2020b), fatalities increase and welfare loss
86 (Dottori et al., 2018)), and humans’ feedback on the Earth system, such as those from
87 climate mitigation on water and food security (Cheng et al., 2022; Fujimori et al., 2022).

88 ~~However, global–~~

89 ~~Currently, most CHANS models cannot represent the complex dynamics of~~
90 ~~human–natural interactions~~are at the global scale (Calvin and Bond-Lamberty, 2018)
91 ~~with much fewer regional models. While global modeling research has deepened our~~
92 knowledge of dynamic feedbacks among Earth’s spheres and system evolution under
93 climate change, sustainability challenges often manifest at regional scales, where social
94 and ecological dynamics are more intricately intertwined (Liu et al., 2007). Compared
95 to global CHANS, regional CHANS are open systems that continuously exchange
96 energy and materials with other regions and the global system, e.g., water resources and
97 electricity transfers (Dobbs et al., 2023; Zhang et al., 2022a) and trade (Ristaino et al.,
98 2021), resulting in pericoupling and telecoupling of different systems (Liu, 2017).
99 Besides, regional CHANS are shaped by more immediate and complex human
100 influences and stressors, such as urban expansion (van Vliet, 2019), ecological
101 protection (Xu et al., 2017; Yang et al., 2022), and water resource regulation policies
102 (diversion and allocation) (Song et al., 2024), which alter regional CHANS dynamics.
103 ~~level, due to the openness of regional CHANS, diversified regional human and natural~~
104 ~~processes, with locally~~Due to their diverse ecological and socioeconomic resilience,
105 regional CHANS exhibit heterogeneous responses to external weather events and
106 climate change, as evidenced by differing responses in crop yield (Hasegawa et al.,
107 2021) and economic production to extreme heat and warming (Waidelich et al.,
108 2024a) disturbances. Moreover, Furthermore, the coarse spatiotemporal resolution of
109 global models limits their capacity to support effective decision-making for regional
110 development (X. Li et al., 2018). As such, advancing regional CHANS modeling is

111 essential for informing adaptive strategies in the face of growing regional
112 environmental and societal pressures.

113 To address this limitation, many regional CHANS models have been developed at
114 various regional scales (e.g., national, basin, and urban) using System Dynamics (SD)
115 and agent-based modeling (ABMs) techniques. Notable examples include the ANIME-
116 Yangtze model (Jiang et al., 2022), the T21-China (Qu et al., 2020), and the iSDG-
117 Australia model (Allen et al., 2019), all based on SD, the Jordan Water Model (Yoon et
118 al., 2021) based with its core on ABM, as well as integrated models in the San Juan
119 River Basin (Hyun et al., 2019) and the Heihe River Basin (Li et al., 2021). These
120 models are designed to capture finer-scale dynamics and region-specific human–natural
121 interactions, since they embed localized characteristics (e.g., fishing ban, reservoir
122 operation strategies, demographic policies, transboundary flows) and account for
123 heterogeneity overlooked by global models. As a result, regional CHANS models offer
124 stronger policy relevance, providing actionable insights for national, basin, and urban
125 decision-making, and advancing CHANS research across multiple scales.

126 The Yellow River Basin (YRB) in China is one of the regions where conflicts
127 between human and natural systems are most acute and complex, particularly in terms
128 of human–water relations, due to the severe imbalance between socioeconomic
129 development and natural hydrological, ecosystem processes. The YRB faces severe
130 water stress, with the water resource utilization rate exceeding 80% (Feng and Zhu,
131 2022; Zhang et al., 2022b). Intensive water extraction has triggered a series of
132 ecological and environmental issues, including flow interruptions, water pollution, and
133 declining groundwater levels, all of which in turn constrain socioeconomic
134 development. The Yellow River traverses the Loess Plateau (Zhu et al., 2019), where
135 severe soil erosion makes the Yellow River one of the most sediment-laden rivers
136 globally (Fu et al., 2011; Yin et al., 2021). The pronounced spatial and temporal
137 variability in streamflow and sediment load leads to significant riverbed aggradation,
138 frequent flooding, and disruption of agricultural production and other livelihood

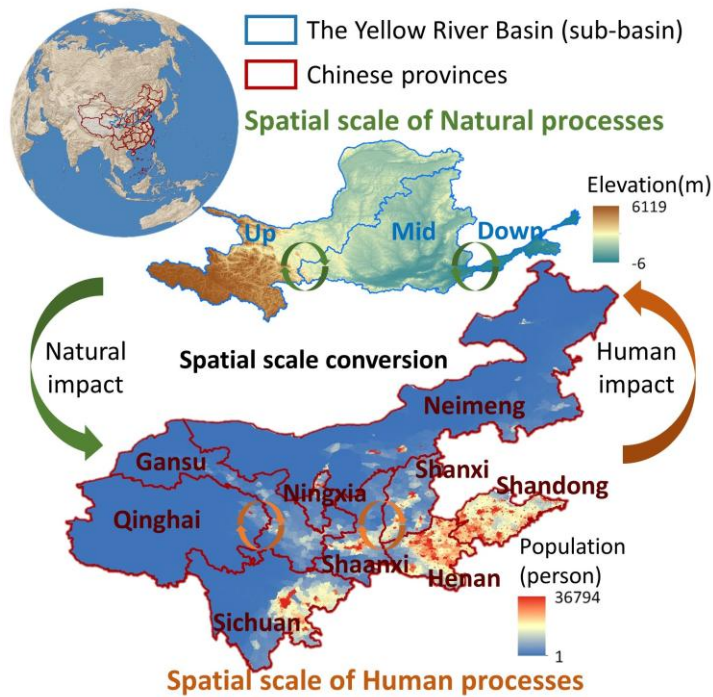
139 activities (Miao et al., 2016). Due to internal hydrological connectivity, sub-basins are
140 highly interconnected and are susceptible to upstream influences. Upstream water
141 overuse diminishes downstream availability (Wei et al., 2023), a factor that played a
142 major role in flow interruptions during the 1990s (Changming and Shifeng, 2002; Wang
143 et al., 2019). Ecological challenges differ across the subbasin, with the upstream facing
144 ecosystem degradation and limited water retention (Ning et al., 2022), the midstream
145 characterized by soil erosion and large-scale ecological restoration (Fu et al., 2011), and
146 the downstream focusing on wetland conservation (Fu et al., 2023). Policy measures
147 aimed at ecological restoration, such as afforestation and cropland conversion, have
148 increased vegetation cover, reduced sediment loads but also decreased runoff,
149 exacerbating water scarcity (Feng et al., 2016; Wang et al., 2016). These interlinked
150 dynamics underscore the YRB as a complex coupled human–natural system, where
151 addressing environmental challenges requires an integrated, systems-oriented approach.

152 The existing models for the YRB are typically designed for specific problems with
153 a narrow application focus and only represent a limited set of human and natural
154 components within the CHANS. These include limited nature-to-human impact
155 pathways, e.g., low flows threatening farmers' livelihoods (Liu et al., 2008), the damage
156 of floods and droughts on agriculture (Zhang et al., 2015), as well as human-to-nature
157 impact pathways, e.g., effects of ecological restoration policy on hydropower and
158 water–sediment–carbon dynamics (Wu et al., 2025; Yan et al., 2024), and the impacts
159 of irrigation water-saving and salinity-control practices on crop yield and water
160 productivity (Wu et al., 2023). These models focus on isolated components of CHANS,
161 with limited consideration of fully coupled human–natural interactions, which limits
162 their capacity to represent full human–natural interactions and support regional
163 decision-making.

164 To address the gap in CHANS modeling for the YRB, following our previously
165 proposed CHANS modeling framework for the basin (Sang et al., 2025b), we
166 implemented the framework to develop the coupled human and natural systems model

167 for the YRB (CHANS-SD-YRB) using the System Dynamics approach. Through
 168 dynamic interaction with policies, climate change, human activities, and environmental
 169 feedbacks, the CHANS-SD-YRB model provides a platform for predicting system
 170 dynamics, conducting scenario analyses, evaluating policies, and optimizing water-
 171 food-carbon synergies. This study offers both theoretical and practical insights for
 172 advancing regional CHANS modeling and promoting sustainable development in the
 173 YRB.

174 **2 Description of the CHANS-SD-YRB**

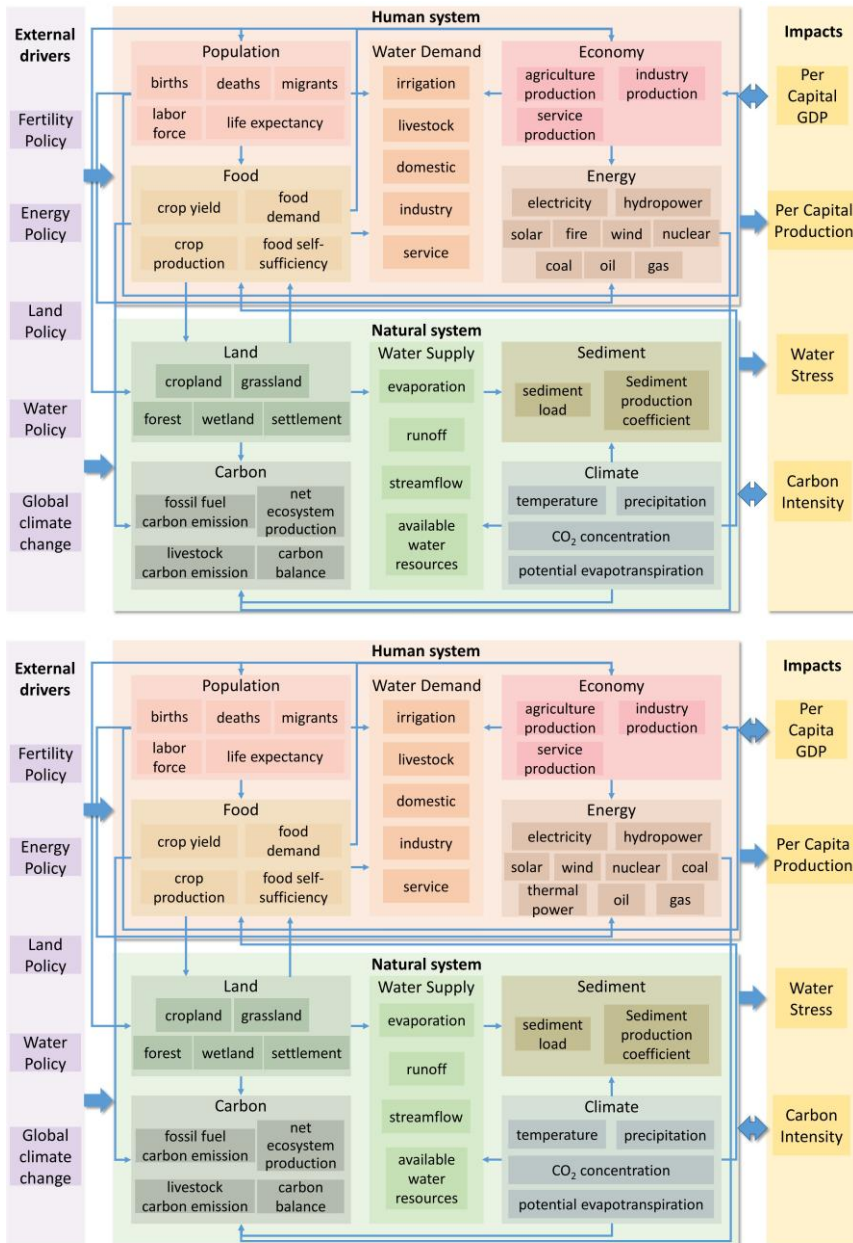


175
 176 Fig.1 Geolocation of the Yellow River Basin and boundary of the natural and human
 177 processes in the CHANS-SD-YRB model. Natural processes are simulated at the sub-
 178 basin scale (base map: elevation), and human processes at the provincial scale across
 179 nine provinces (base map: population density in 2020).

180 We developed the CHANS-SD-YRB based on system dynamics, a method well-

181 suited for capturing complex system behaviors characterized by nonlinearity, multi-
182 level structures, and feedback loops (Forrester, 1968; Richardson, 2011). The model
183 was constructed and implemented using the VENSIM DSS (Ventana Systems, 2023)
184 software platform, operating on an annual time step. The CHANS-SD-YRB simulates
185 both human and natural processes for historical simulations (1981–2020) and future
186 projections (2021–2100). Human processes are simulated at the provincial scale,
187 covering the nine provinces along the Yellow River (Qinghai, Sichuan, Gansu, Ningxia,
188 Neimeng, Shaanxi, Shanxi, Henan, and Shandong), while natural processes are
189 simulated at the sub-basin scale (up-, mid-, and downstream) (Fig.1). The model is
190 designed to capture the various interactions within and between different components
191 of human system and natural system across administrative and hydrological units. The
192 spatial scale conversion between provincial and sub-basin levels relies on weights (e.g.,
193 the proportion of sub-basin-level values to provincial total values) derived from
194 historical high-resolution gridded datasets of human-related variables. These weights
195 enable disaggregation of provincial outputs to the sub-basin level (see Supporting
196 Information S4 for details). Given the availability of gridded data for human processes
197 and the strong correlations among relevant variables, gridded population and GDP data
198 were used as proxies to disaggregate demographic variables and economic and human
199 carbon emissions, respectively, from provincial-level ~~outputs~~ to the sub-basin scale
200 (Table S3).–

201 **2.1 Model structure**



202

203

204 Fig.2 Structure of the CHANS-SD-YRB, which shows sectors of human and natural
 205 systems, their key processes and interactions.

206 Drawing on the modeling framework of CHANS in the YRB (Sang et al., 2025b),
207 we designed the CHANS-SD-YRB structure (Fig. 2), including five sectors related to
208 human society (*Population, Economy, Energy, Food, and Water Demand*), and five
209 sectors related to natural ecosystem (*Water Supply, Sediment, Land, Carbon, and*
210 *Climate*).

211 These sectors are interconnected to represent various human-natural interactions
212 as summarized below. Key interactions among human system modules are summarized
213 below. The *Population* sector affects food demand (*Food*), residential water use (*Water*
214 *Demand*), household electricity and gas consumption (*Energy*), and settlement land area
215 (*Land*). The sector also interacts dynamically with the *Economy* sector, where economic
216 output influences deaths and migrants, while the labor force, in turn, drives economic
217 production. The *Economy* sector drives energy uses (electricity, coal, oil, and gas use)
218 from *Energy*, as well as industrial and service water withdrawal from *Water Demand*.
219 The gross agricultural production in the *Economy* is made up of crop and livestock
220 production (*Food*). The *Energy* sector produces fossil fuel emissions in the *Carbon*
221 sector. The *Food* sector is affected by the *Land* and *Climate* sector, and it also
222 determines irrigation water withdrawal (*Water Demand*) and livestock-related
223 emissions (*Carbon*). Additionally, the *Food* sector interacts closely with the *Land* sector,
224 where crop production depends on cropland area, which, in turn, is influenced by food
225 self-sufficiency. The *Water Demand* sector affects streamflow in the *Water Supply*
226 sector through consumptive water use.

227 The key interactions among natural system modules are listed below. The *Land*
228 sector influences evapotranspiration in the *Water Supply* sector through vegetation
229 coverage, and it influences carbon absorption in *Carbon* sector through land use area.
230 The carbon absorption is also affected by climatic variables including temperature,
231 precipitation, and CO₂ concentration. Similarly, runoff in the *Water Supply* sector is
232 affected by precipitation, precipitation intensity (mm/h, the rate of rainfall within one
233 hour calculated from daily data), and potential evapotranspiration. Streamflow

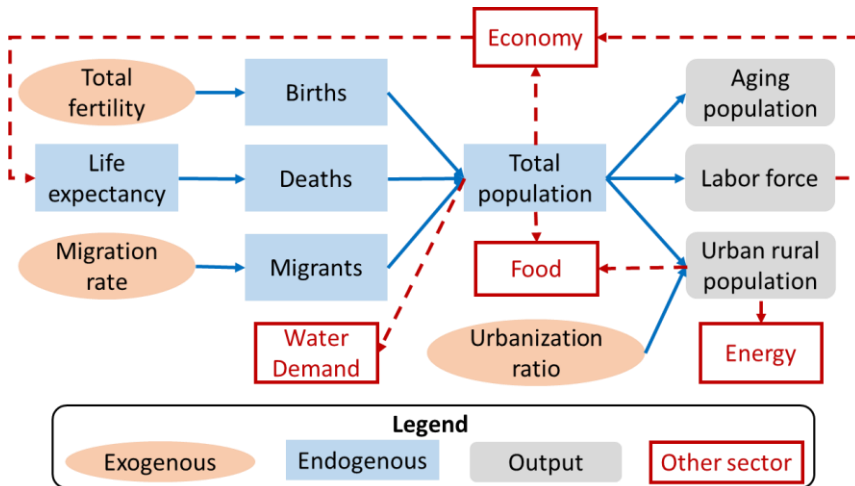
234 influences sediment dynamics in the *Sediment* sector together with the *Climate* sector.

235 In addition, the CHANS dynamics in the YRB are modulated by external drivers,
236 including policies and global climate change that affect various modeled processes (e.g.,
237 fertility, energy, land use, and water). With comprehensive representation of CHANS
238 processes and their interactions, the CHANS-SD-YRB model is capable of generating
239 integrated indicators to assess the state of the coupled system, such as per capita GDP,
240 per capita food production, water stress, and carbon intensity. These indicators not only
241 serve as evaluation metrics but also feed back to influence the internal dynamics of the
242 human–natural system in the YRB.

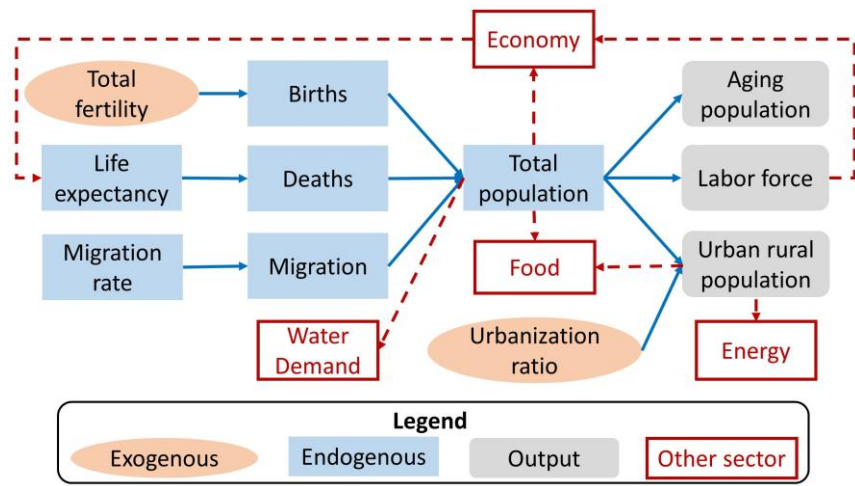
243 **2.2 Sector description**

244 The CHANS-SD-YRB model focuses on the essential human–natural processes in
245 the YRB, with a particular emphasis on human–water interactions. To this end, it has a
246 comprehensive representation of the full range of natural and human processes that
247 influence water use and supply. Formulation of each sector aims to explicitly account
248 for cross-sectoral interactions as fully as possible while remaining sufficiently simple
249 to be implemented within the SD software. Considering data availability and the spatial
250 scales of process, human sectors (*Population, Economy, Energy, Food, and Water*
251 *Demand*) are simulated at the provincial level, while natural sectors (*Water Supply,*
252 *Sediment, Land, Carbon, and Climate*) are simulated at the sub-basin level within the
253 YRB. Next, we describe each sector and its key formulation and provide full details in
254 Supporting Information S2.

255 **2.2.1 Population**



256



257

258 Fig.3 Structure of the *Population* sector. Blue lines indicate connections inside the
 259 sector, red dotted lines indicate connections with other sectors.

260 Population dynamics are ~~represented by birth, death, and migrants, which are~~
 261 ~~determined by a series of social and economic factors driven by births, deaths, and~~
 262 ~~migration (Fig. 3). Births are calculated based on exogenous total fertility rates derived~~
 263 ~~from historical data (Equation S2) to reflect the strong influence of China's Family~~
 264 ~~Planning Policy. Deaths are determined by the life expectancy, which is modeled as a~~

265 function of human well-being (Equations S3-S6). Migration is calculated based on
 266 historical statistical data and per capita GDP differences between YRB and the national
 267 average level (Equations S7-S8). The total population is characterized by age and
 268 gender with exogenous urbanization ratios. The output of *Population* sector drives
 269 *Economy, Energy, Food, and Water Demand* sectors through labor force, urban and
 270 rural populations.

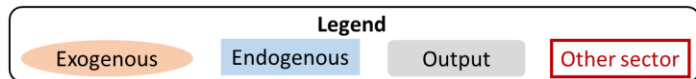
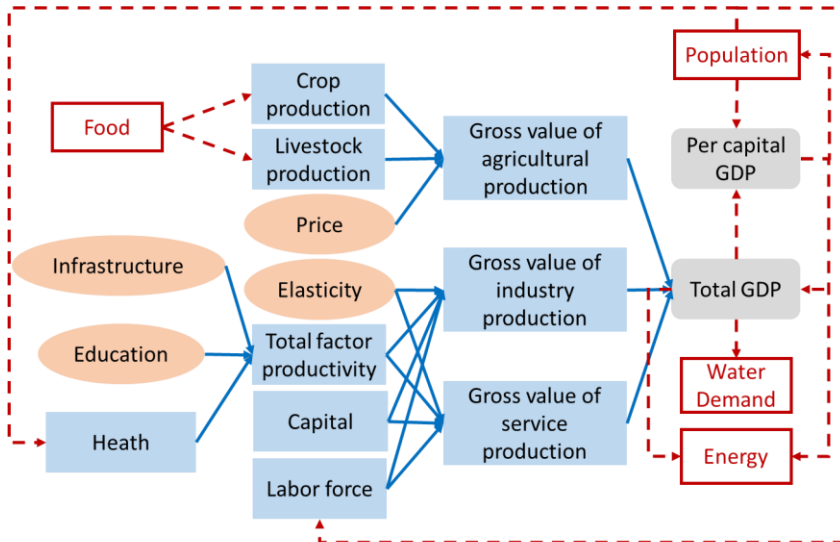
271 The key variable, total population, is modeled using the age-structured
 272 mathematical method (Kemei et al., 2024), which categorizes individuals by one-year
 273 age group and gender (Equation 1),

$$274 \text{Pop}_{g,a} = \text{IniPop}_{g,a} + \begin{cases} \int (B_{g,a} + NM_{g,a} - D_{g,a})dt, & a = 0 \\ \int (\text{Pop}_{g,a} + NM_{g,a} - D_{g,a})dt, & 1 \leq a \leq 99, a = 100 \text{ and over} \end{cases}$$

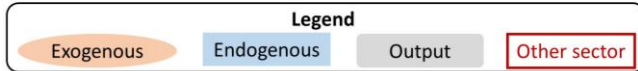
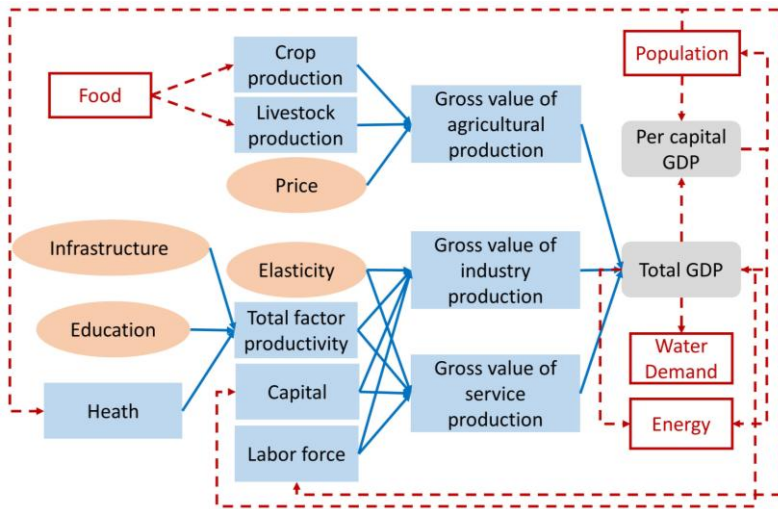
275 (1)

276 where *Pop* is population, subscript *g* and *a* are gender (*g* = M is male, *g* = F is female)
 277 and age (*a* = 0-100 and over); *IniPop*_{*g,a*} is the population in the initial year, *B*_{*g,a*} is the
 278 births ~~(Equation S2)~~, *D*_{*g,a*} is the deaths ~~(Equations S3-S6)~~, and *NM*_{*g,a*} is the net
 279 migrants (i.e., immigrants – emigrants, ~~Equations S7-S8~~).

280 **2.2.2 Economy**



281



282

283 Fig.4 Structure of the *Economy* sector. Blue lines indicate connections inside the

284 sector, red dotted lines indicate connections with other sectors.

285 The *Economy* sector simulates production activities in agriculture, industry, and
286 services, which in turn drive changes in the *Population*, *Energy*, and *Water Demand*
287 sectors- (Fig. 4).

288 The gross product of industry and services is calculated using the Cobb-Douglas
289 production function (Cobb and Douglas, 1928) to account for multiple factors in the
290 economy (Equation 2). Exogenous variables (infrastructure, education, and elasticity),
291 and endogenous variables (health and labor force) from the *Population* sector
292 (Equations S10-S17S21) all affect the gross domestic product in industry and service
293 (GDP_s),

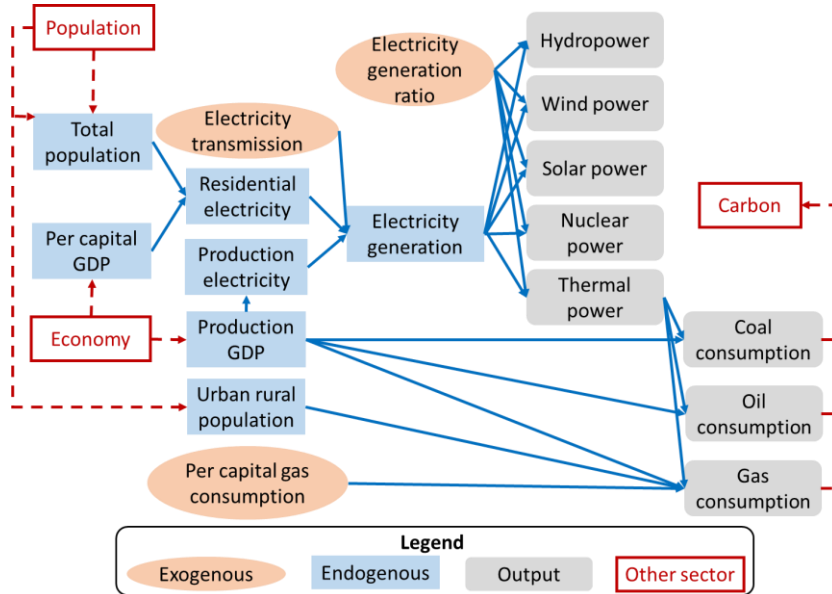
$$294 \quad GDP_s = IniGDP_s \times TFP_s \times \left(\frac{L_s}{IniL_s}\right)^{1-\alpha_s} \times \left(\frac{K_s}{IniK_s}\right)^{\alpha_s} \quad (2)$$

295 where subscript s represents industry and service, $IniGDP_s$ is the initial GDP; TFP_s is
296 the total factor productivity; calculated from exogenous (infrastructure, education, and
297 elasticity) and endogenous variables (health and labor force) (Equations S10-S13); L_s
298 represents the labor force and $IniL_s$ is its initial value (from *Population* sector); α_s is and
299 1- α_s are capital and 1- α_s is labor elasticities, from T21-China (Qu et al., 2020); and
300 calibrated using historical data; K_s and $IniK_s$ refer to the capital stock and its initial level.

301 Gross agricultural production includes crop and livestock production from *Food*
302 sector, calculated by their respective prices (Equations S18-S19S22-S23).

带格式的：允许文字在单词中间换行

303 2.2.3 Energy

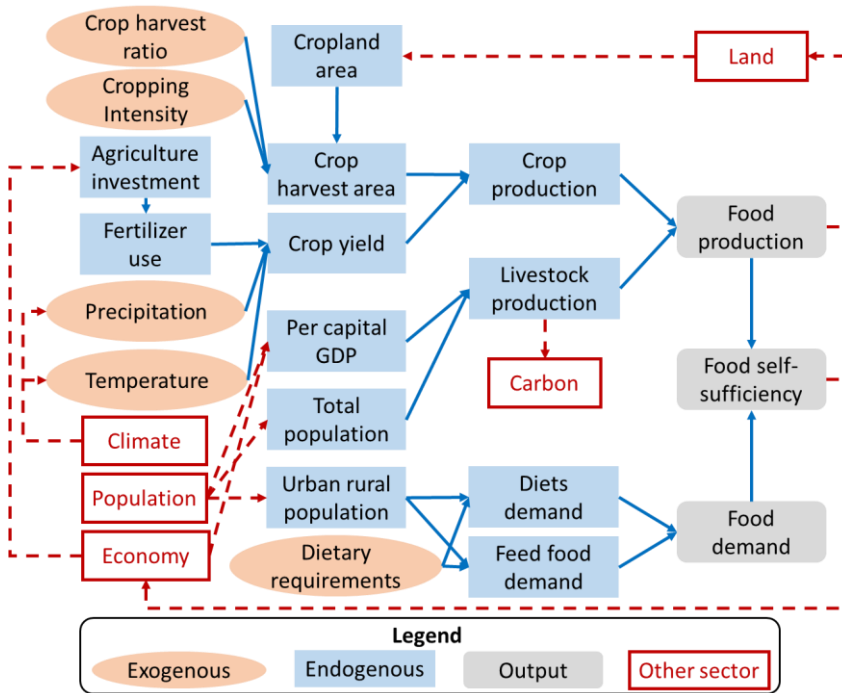


304
305 Fig.5 Structure of the Energy sector. Blue lines indicate connections inside the sector,
306 red dotted lines indicate connections with other sectors.

307 The Energy sector simulates production, consumption, and the structure of the
308 energy system, encompassing fossil fuels (coal, oil, and gas) and electricity. ~~Coal, oil,~~
309 ~~(Fig. 5). Energy production and gas consumption are derived from linear relationships~~
310 ~~between historical sectoral GDP and corresponding consumption (Equations S22-~~
311 ~~S24) always balanced in this sector.~~ Electricity generation is divided into residential
312 and industrial production uses, the former is estimated from the linear fit of historical
313 per capita GDP and residential demand, and the latter is calculated using GDP and
314 electricity intensity data from the China Energy Statistical Yearbook (NBSC, 2020a)
315 (Equations S20-S21S24-S25). Cross-provincial electricity transmission is also
316 incorporated according to the same yearbook. The shares of electricity generated from
317 thermal, hydro, wind, solar, and nuclear sources are determined by exogenously
318 specified ratios, as reported in the China Energy Statistical Yearbook (NBSC, 2020a).
319 ~~Fossil~~The fossil fuel consumption drives by economic production of industry and

320 service sectors is modeled as a linear function of sectoral GDP based on historical data
 321 (Equations S26-S28). It combines with fossil fuel consumption for electricity
 322 generation and residential gas consumption to drive carbon emissions in the Carbon
 323 sector.

324 **2.2.4 Food**



325
 326 Fig.6 Structure of the Food sector. Blue lines indicate connections inside the sector,
 327 red dotted lines indicate connections with other sectors.

328 The Food sector simulates the production of livestock and crops, and food demand,
 329 and these productions directly affect gross agricultural production in the Economy
 330 sector. (Fig. 6). Livestock production ($Livestock_{pro}$) is calculated by an empirical
 331 function, driven by economic development and population growth (Equation 3),

332
$$Livestock_{pro} = Pop \times \left(Para_{GL1} + (Para_{GL2} - Para_{GL1}) \times \frac{PC_{GDP}}{PC_{GDP} + Const_{GL}} \right) \quad (3)$$

333 where $Para_{GL1}$, $Para_{GL2}$ and $Const_{GL}$ are parameters obtained by fitting the historical
 334 per capita meat production and per capita GDP (PC_{GDP}) data.

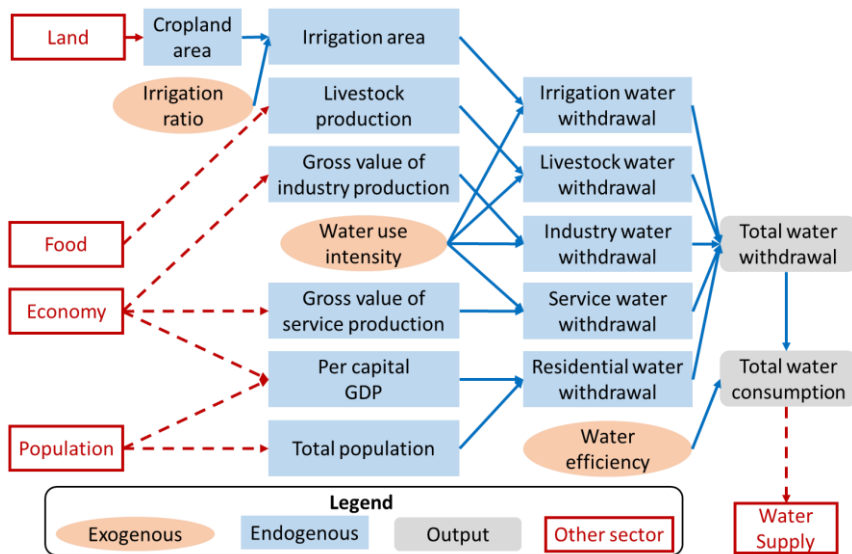
335 Crop production ($Crop_{pro}$) is determined by the yield ($Yield_c$) and harvest area (PA_c)
 336 of seven major crop types (subscript c): rice, wheat, corn, soybeans, cotton, potatoes,
 337 and oil crops (Equation 4). The harvest area is influenced by cropland area from the
 338 *Land* sector, exogenous cropping intensity and crop harvest ratio. Crop yields are
 339 positively affected by agricultural investment from the *Economy* sector, along with
 340 effects of precipitation, temperature, and CO₂ concentration from the *Climate* sector
 341 (Equations ~~S26-S31~~S30-S36).

342
$$Crop_{pro} = \sum_{c=1}^7 Yield_c \times PA_c \quad (4)$$

带格式的: 允许文字在单词中间换行

343 Food demand encompasses both staple and feed grain demand, which are
 344 determined by population size from *Population* sector and dietary patterns (Equations
 345 ~~S33-S36~~S37-S41).

346 **2.2.5 Water Demand**



347
 348 Fig.7 Structure of the *Water Demand* sector. Blue lines indicate connections inside the
 349 sector, red dotted lines indicate connections with other sectors.

350 The *Water Demand* sector simulates water withdrawal (WW) and consumption
 351 (WC) across multiple uses—irrigation, livestock, industry, services, and residential—

352 in the nine provinces of the YRB- (Fig. 7). Water consumption is derived as the product
353 of water withdrawal and water use efficiency reported in the Water Resources Bulletin
354 (YRCCMWR, 2020) (Equations S37-S38, S42-S43), which affects the *Water Supply*
355 sector.

356 Irrigation water withdrawal (WW_{irr}) is estimated through a physically-based
357 on function of exogenous irrigation water use intensity (WWI_{irr}), and cropland irrigation
358 cropland ratios (IR) from the China Agricultural Yearbook (MAARA, 2020), and
359 cropland area ($Area_{Cropland}$) provided by the *Land* sector (Equation 5).

$$360 \quad WW_{irr} = WWI_{irr} \times Area_{Cropland} \times IR \quad (5)$$

带格式的: 允许文字在单词中间换行

361 The water withdrawal for livestock, industry, and services is also driven by
362 exogenous sectoral water use intensities collected from the China Statistical Yearbook
363 and National Long-term Water Use Dataset of China (Zhou et al., 2020), in combination
364 with livestock production from the *Food* sector, economic output from the *Economy*
365 sector (Equations S40-S43, S45-S48).

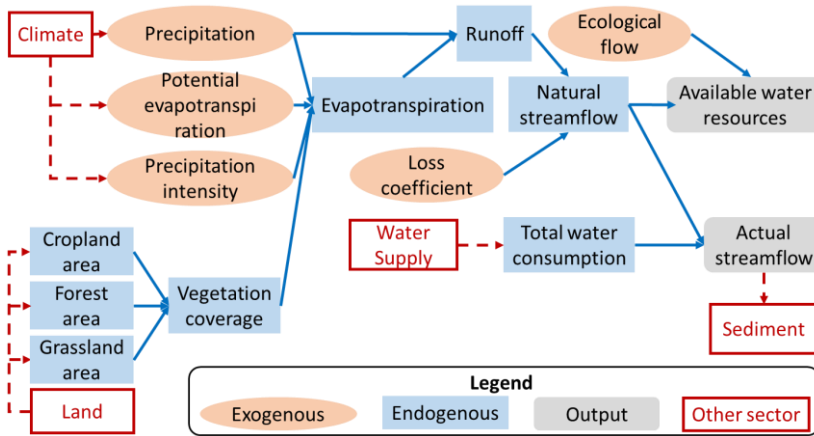
366 Residential water withdrawal (WW_{res}) is obtained derived from the a non-linear
367 empirical function, driven by of economic development and population growth with an
368 upper limit of per capita domestic water use (Flörke et al., 2013) because water demand
369 per person cannot increase indefinitely (Equation 6),

$$370 \quad WW_{res} = Pop \times \left(Para_{GD1} + (Para_{GD2} - Para_{GD1}) \times \frac{PC_{GDP}}{PC_{GDP} + Const_{GD}} \right) \quad (6)$$

带格式的: 允许文字在单词中间换行

371 where $Para_{GD1}$, $Para_{GD2}$, and $Const_{GD}$ are parameters obtained by fitting the historical
372 per capita domestic water use with per capita GDP (PC_{GDP}).

373 **2.2.6 Water Supply**



374
375 Fig.8 Structure of the *Water Supply* sector. Blue lines indicate connections inside the
376 sector, red dotted lines indicate connections with other sectors.

377 The *Water Supply* sector simulates runoff, discharge, and their changes in each
378 sub-basin- (Fig. 8). Runoff (R) is determined by precipitation (Pre) and
379 evapotranspiration (ET) based on the water balance principle derived from the Budyko
380 equation, which is suitable for non-humid regions of China (Yang et al., 2009)
381 (Equation 7).

382
$$R = Pre - ET \quad (7)$$

383 The ET is calculated by various exogenous climate variables from the *Climate*
384 sector, and vegetation coverage from the *Land* sector (Equations 8-9, S46-S48S51-S53),

385
$$ET = \frac{PET \times Pre}{(Pre^n + EP^n)^{\frac{1}{n}}} \quad (8)$$

386
$$n = Para_{E1} \times \left(\frac{Ks}{PI}\right)^{Para_{E2}} \times FVC^{Para_{E3}} \times e^{Para_{E4} \tan \beta} \quad (9)$$

387 where PET is potential evapotranspiration at sub-basin, from the *Climate* sector; n is a
388 parameter reflecting the basin landscape characteristics, related to saturated hydraulic
389 conductivity (Ks), precipitation intensity (PI), average slope (β), and fraction of
390 vegetation coverage (FVC); $Para_{E1}$, $Para_{E2}$, $Para_{E3}$, and $Para_{E4}$ are parameters fitted
391 from historical data.

带格式的：允许文字在单词中间换行

带格式的：允许文字在单词中间换行

392 Runoff and the loss coefficient (defined by the ratio of natural streamflow to runoff)
 393 determine the natural streamflow due to the water loss during the confluence process
 394 (Equation S49S54). Natural streamflow and ecological flow constraints define the
 395 upper limit of available water resources. By integrating human water consumption from
 396 the *Water Demand* sector across sub-basins, the model calculates the actual streamflow
 397 (Equations S50-S52S55-S57). Actual streamflow is transferred through hydrological
 398 connectivity from upstream to midstream and then to downstream, ultimately reaching
 399 the sea, which governs sediment transport processes within the *Sediment* sector.

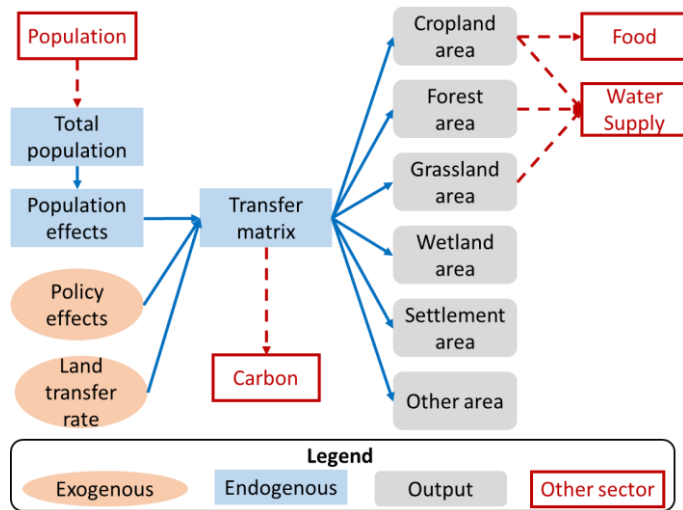
400 2.2.7 Sediment

401 The *Sediment* sector estimates sediment load (*Sed*) for each sub-basin using an
 402 empirical model in the literature (Yin et al., 2023b), which links actual streamflow from
 403 the *Water Supply* sector to sediment transport,

$$404 \quad Sed = Para_{SS} \times AS + Const_{SS} \quad (10)$$

405 where *Parass* and *Constss* are derived from linear fitting of historical hydrological
 406 station data on actual streamflow and sediment load.

407 2.2.8 Land



408
 409 Fig.9 Structure of the *Land* sector. Blue lines indicate connections inside the sector,

410 red dotted lines indicate connections with other sectors.

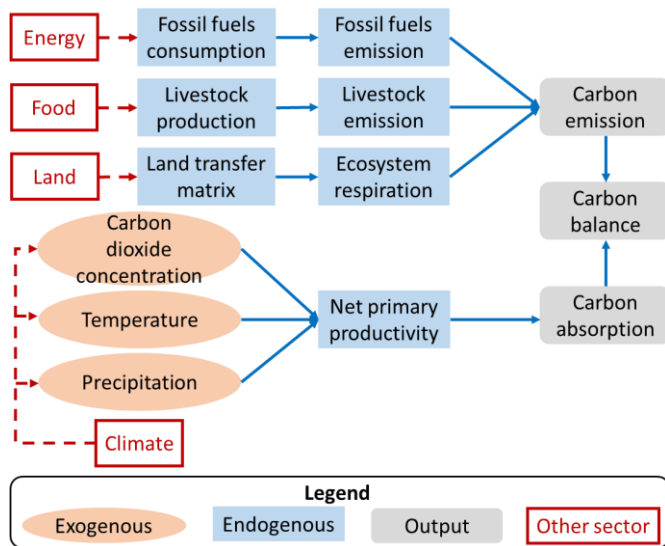
411 The *Land* sector simulates the area changes of six land use types (cropland, forest,
 412 grassland, wetland, settlement, and others) based on the land transfer matrix obtained
 413 from historical remote sensing data (Xu et al., 2018). The land transfer matrix calculates
 414 the inflow and outflow of each land category and can be configured to represent the
 415 influence of future land use drivers- (Fig. 9). This sector outputs vegetation area
 416 (including forest, grassland, and cropland), which influences the *Water Supply* sector.
 417 Cropland area changes impact the *Food* sector, while land use conversion also plays a
 418 role in the *Carbon* sector.

419 Based on the initial land use area ($IniArea_i$), the transfer matrix determines the area
 420 ($Area_i$) allocated to each land use type (Equations 11, S55-S6+S60-S66),

$$421 \quad Area_i = IniArea_i + \int (\sum_{i=1}^6 FTM_{i,j} - \sum_{j=1}^6 FTM_{i,j}) dt \quad (11)$$

422 where $FTM_{i,j}$ is the final land use transfer matrix, indicating the area of land use i
 423 transferred to land use j , i and j represent six land use type.

424 **2.2.9 Carbon**



425
 426 Fig.10 Structure of the *Carbon* sector. Blue lines indicate connections inside the

427 sector, red dotted lines indicate connections with other sectors.

428 The *Carbon* sector simulates the basin's carbon balance processes, including
429 carbon emission and absorption, adapted from the carbon cycle of ANEMI (Davies and
430 Simonovic, 2011). Carbon emissions (*CE*) encompass fossil fuel emissions, and
431 livestock emission, and ecosystem respiration, which are influenced by outputs from
432 the *Energy*, *Food*, and *Land* sectors- (Fig. 10).

433 Fossil fuel and livestock emissions are calculated based on fossil fuel consumption,
434 livestock production, and their respective emission coefficients. Ecosystem emissions
435 include carbon released from burning as well as from the decomposition of biomass,
436 litter, humus, and charcoal, which are determined by carbon pools' lifespans,
437 decomposition factor, and respiration coefficients (Equations S64-S88S67-S93).

438 Carbon absorption (*CA*) is determined by net primary productivity (*NPP*) and land
439 use area. *NPP* is influenced by climate factors, including CO₂ concentration,
440 temperature, and precipitation (Equations 12, S63),

441
$$CA = \sum_{i=1}^6 NPP_i \times Area_i \quad (12)$$

442 where *i* represent land use type, land use area (*Area_i*) from the *Land* sector.

443 2.2.10 Climate

444 The *Climate* sector supplies both historical and projected climate data essential for
445 the *Water Supply*, *Food*, and *Carbon* sectors. The key climate variables comprise
446 temperature and precipitation (at the sub-basin and provincial levels), as well as
447 potential evapotranspiration, precipitation intensity, and CO₂ concentration (at the sub-
448 basin level). These variables are treated as exogenous inputs, without accounting for
449 potential feedbacks from human activities or natural system responses on regional
450 climate patterns.

451 2.3 Data sources

452 In the model, there are more than 100 exogenous variables, some of which are
453 initial variables that drive the simulation. These exogenous variables are derived either
454 from historical statistical data or from fitted results based on historical data (Table S2).

455 All data sources required for the model simulation are listed in Table 1.

456 Table 1. Summary of data sources for the YRB model. Updated from Sang et al.

457 (2025).

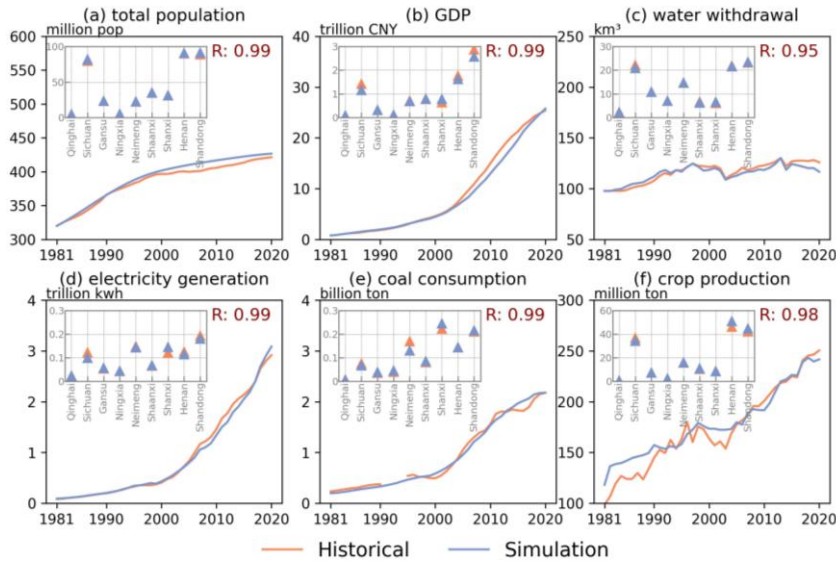
Sector	Variables*	Data sources	Spatial and temporal scale	Time range
Population	age-specific population, births, deaths, migrants	<ul style="list-style-type: none"> China Statistical Yearbook (NBSC, 2020c), China Population Census Yearbook (NBSC, 2020b) 	<ul style="list-style-type: none"> provincial, annual 	<ul style="list-style-type: none"> 1981–2023
Economy	GDP, investment, employment	<ul style="list-style-type: none"> China Agricultural Yearbook (MAARA, 2020), China Statistical Yearbook (NBSC, 2020c) 	<ul style="list-style-type: none"> provincial, annual 	<ul style="list-style-type: none"> 1981–2023
Energy	electricity, coal, oil, gas consumption	<ul style="list-style-type: none"> China Energy Statistical Yearbook (NBSC, 2020a) 	<ul style="list-style-type: none"> provincial, annual 	<ul style="list-style-type: none"> 1981–2023
Food	crop production, fertilizer, irrigated area	<ul style="list-style-type: none"> China Agricultural Yearbook (MAARA, 2020) 	<ul style="list-style-type: none"> provincial, annual 	<ul style="list-style-type: none"> 1981–2023
Water demand	Industrial, domestic, irrigation water withdrawal	<ul style="list-style-type: none"> National Long-term Water Use Dataset of China (NLWUD) (Zhou et al., 2020) China Statistical Yearbook (NBSC, 2020c) 	<ul style="list-style-type: none"> prefectural, annual 	<ul style="list-style-type: none"> 1965–2013 1981–2023
Water supply	runoff, streamflow, water stress	<ul style="list-style-type: none"> China Natural Runoff Dataset (CNRD) (Gou et al., 2021), Gauge-based Natural Streamflow Dataset (Miao et al., 2022) Yellow River Water Resources Bulletin (YRCCMWR, 2020) 	<ul style="list-style-type: none"> 0.25° grid, Monthly 0.25° grid, annual provincial, annual 	<ul style="list-style-type: none"> 1961–2018 1961–2018 1998–2022
Sediment	sediment load	<ul style="list-style-type: none"> Yellow River Water 	<ul style="list-style-type: none"> provincial, 	<ul style="list-style-type: none"> 1998–2022

		Resources Bulletin (YRCCMWR, 2020)	annual	
Land	cropland, forest, grassland, wetland, settlement	<ul style="list-style-type: none"> China land use remote sensing monitoring dataset (CNLUCC) (Xu et al., 2018) Long-term global land surface satellite fractional vegetation cover product (Jia et al., 2015, 2019) 	<ul style="list-style-type: none"> 1 km grid, annual 	<ul style="list-style-type: none"> 1980, 1990, 1995, 2000, 2005, 2010, 2015, 2020
Carbon	fossil fuel carbon emissions, net primary productivity	<ul style="list-style-type: none"> Carbon Emission Accounts and Datasets (Shan et al., 2018), Global Vegetation Productivity Products (GVPP) (Cui et al., 2016; Wang et al., 2020a; Yu et al., 2018) 	<ul style="list-style-type: none"> Provincial, annual 5 km grid, 8 day 	<ul style="list-style-type: none"> 1997–2021 1981–2018
Climate	temperature, precipitation, CO ₂ concentration, potential evapotranspiration and precipitation intensity	<ul style="list-style-type: none"> Gridded daily observation dataset over China region (Wu and Gao, 2013), European Environment Agency (EEA, 2019), China Meteorological Data Service Center (https://data.cma.cn/) 	<ul style="list-style-type: none"> 0.25° grid, Annual Global, Annual Meteorological stations, Monthly 	<ul style="list-style-type: none"> 1961–2020 1800-2020 1956-2018

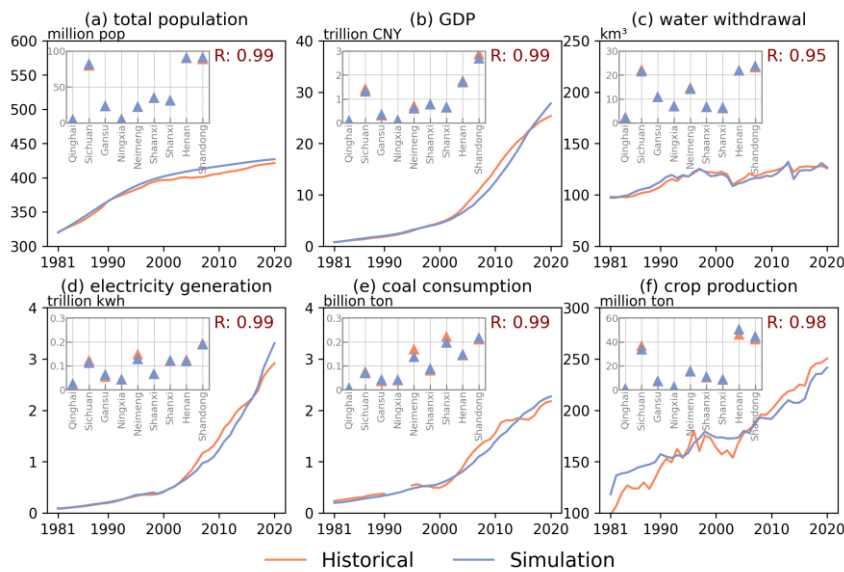
458 * Listed are some typical variables of each sector

459 **3 Model validation and application**

460 **3.1 Historical model validation**



461



462

463 Fig.11 Validation of human system processes during historical period of 1981-2020.

464 (a) total population in *Population* sector; (b) GDP in *Economy* sector; (c) water
 465 withdrawal in *Water Demand* sector; (d) electricity generation and (e) coal

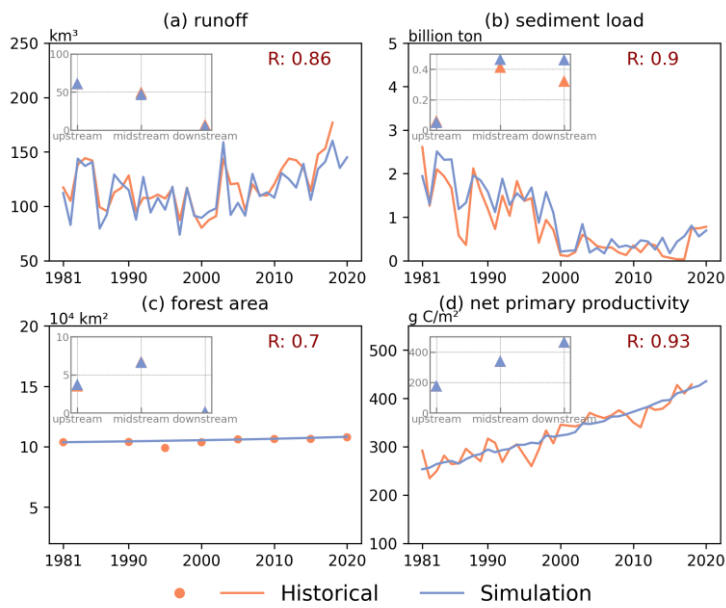
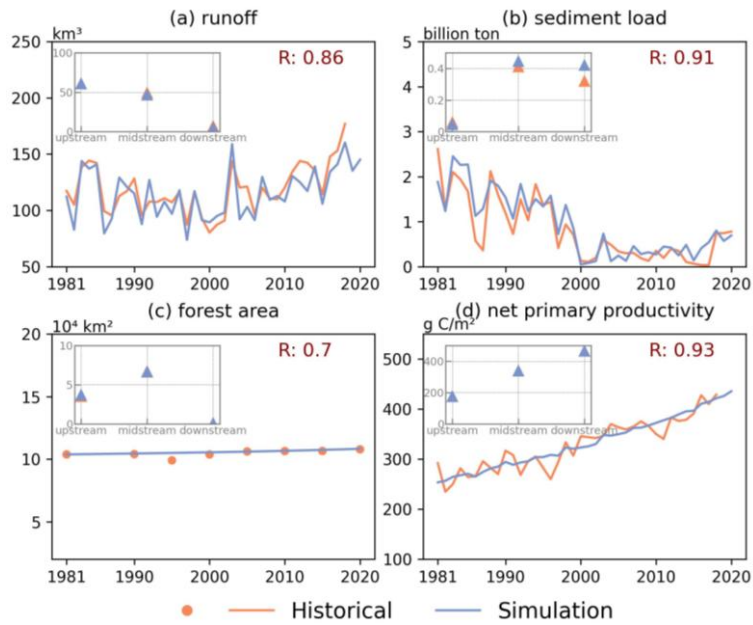
466 consumption in *Energy* sector; (f) crop production in *Food* sector. Pink triangles in the
467 upper left sub-image represents the average of historical and simulation value in
468 1981-2020 of each province in the YRB.

469 We compared model performance during the historical period (1981–2020) against
470 historical data. These data are sourced from multiple channels, including statistical
471 yearbooks, hydrological stations, remote sensing observations, and outputs from other
472 models (Table S3).

473 For human sectors, the simulation accuracy of selected key variables from each
474 sector is consistently high ($R > 0.95$), including total population, gross domestic
475 product (GDP), water withdrawal, electricity generation, coal consumption, and crop
476 production across the nine provinces- (Fig.11). However, the accuracy varies among
477 provinces, particularly for GDP, electricity generation, coal consumption, and crop
478 production. In general, Shanxi exhibits Some provinces, like Neimeng, exhibit lower
479 simulation accuracy compared for certain indicators than others, probably due to the
480 others simplification of relevant modelled processes, imperfect parameterizations, and
481 external policy interventions. Among all sectors, the greatest uncertainty arises in
482 simulating coal consumption, because the absence of a clear historical trend results in
483 poor fitting performance. Nevertheless, the model performs reasonably well in the
484 human sectors, effectively capturing the historical dynamics of human systems in the
485 YRB.

带格式的: 字体颜色: 蓝色

带格式的: 字体颜色: 蓝色



486

487

488 Fig.12 Validation of the natural system processes during historical period of 1981-
 489 2020. (a) runoff in *Water Supply* sector; (b) sediment load in *Sediment* sector; (c)
 490 forest area in *Land* sector, and the historical dataset is discontinuous; (d) net primary
 28

491 productivity in *Carbon* sector. Pink triangles in the upper left sub-image represents
492 the average of historical and simulation value in 1981-2020 of each sub-basin in the
493 YRB.

494 For natural sectors, the simulation accuracy for runoff, sediment load, forest area,
495 and NPP in the YRB is relatively high ($R > 0.7$) (Fig.12). At the sub-basin level, the
496 overall performance is satisfactory; however, the model shows lower accuracy in
497 simulating sediment transport in the mid- and downstream. Compared to the human
498 sectors, the natural sectors generally exhibit lower correlations with historical data,
499 largely due to the simplifications required when modeling physically complex natural
500 processes. Nevertheless, the model is still capable of capturing the historical dynamics
501 of natural processes in the YRB.

502 [Sensitivity analyses with randomly generated parameter values reveal growing](#)
503 [uncertainty in the long-term trajectories of socio-economic and natural variables; the](#)
504 [model maintains behavioral robustness across all runs without catastrophic collapse or](#)
505 [unrealistic oscillations \(see Supporting Information S3 for details\).](#)

506 **3.2 Model application for future projection**

507 **3.2.1 Future baseline scenario**

508 The future baseline scenario represents a trajectory in which existing plans and
509 policies continue to operate without substantial changes in external environments. The
510 development of the baseline scenario primarily relies on variables from the *Population*,
511 *Economy*, *Water Demand*, and *Land* sector based on available government planning
512 documents, historical trends, and other projections (Table 2). [For future projections,](#)
513 [variables or parameters not specified in the table are held constant at historical levels](#)
514 [from their most recent year.](#) Future climate data (2015-2100) are from the ensemble
515 mean of 11 CMIP6 models (ACCESS-CM2, CESM2, CMCC-ESM2, GFDL-ESM4,
516 INM-CM4-8, INM-CM5-0, IPSL-CM6A-LR, MIROC6, MRI-ESM2-0, UKESM1-0-
517 LL, and HadGEM-GC31-LL) (available at
518 <https://cds.climate.copernicus.eu/datasets/projections-cmip6?tab=download>) for the

519 SSP 2-4.5 because this scenario aligns more closely with the climate trends in the YRB.
 520 To ensure temporal consistency, CMIP6 historical climate data (1981–2014) were used
 521 instead of observed historical records. To reduce systemic biases in the raw CMIP6 data,
 522 we applied bias correction using CN05 and ground weather stations observations from
 523 1981 to 2014. By statistically aligning the mean of the CMIP6 data with observation
 524 records, systemic bias is removed while retaining the temporal consistency required for
 525 long-term simulation.

526 We run the model under the future baseline scenario to project the evolution of
 527 CHANS in the basin from 2021 to 2100 (see Supporting Information [S5S6](#) for details
 528 of future scenario design and supplementary spreadsheet for exogenous variables).

529 Table 2 Settings of key variables in the future baseline scenario

Sector	Variables	Future baseline
Population	• Total fertility	• 2024 United Nations Population Projections
	• Gender ratio	• 2024 United Nations Population Projections
	• Average years of schooling	• The national maximum in 2023 (Germany) as the upper limit
	• Urban and rural population ratio	• Analysis and Forecast of Urbanization Trends in China's Modernization by 2020
	• Labor force	• Delay retirement age
Energy	• Electricity generation sources ratio	• Projected provincial-level energy structure meeting China's carbon peaking and carbon neutrality goals (Li et al., 2024)
	• Irrigation intensity	• Irrigation water use intensity declines linearly (1%/yr) to its minimum value.
Water Demand	• Industry, service, livestock water use intensity	• Industry, service and livestock water use intensity declines linearly (1%/yr) to its minimum value.
Land	• Land use area	• <u>Cropland, forest, and grassland are allowed</u>

to be converted into each other, but not to
unused land; unused land can be converted
to the rest land; wetlands are fixed.

◆ Minimum cropland area above the red line
for cropland protection.

• ~~Other lands are allowed to be fully
converted into other categories.~~

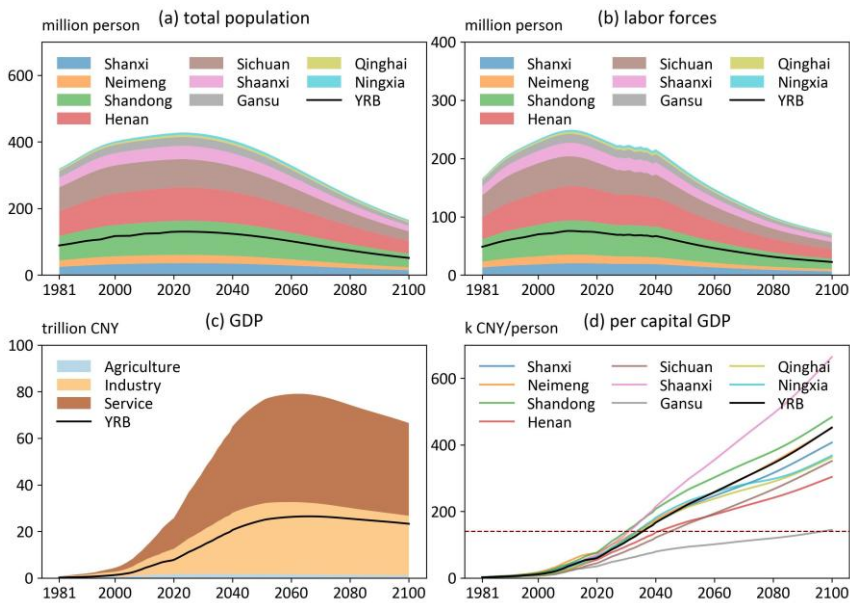
- Temperature
- Precipitation
- Potential

Climate

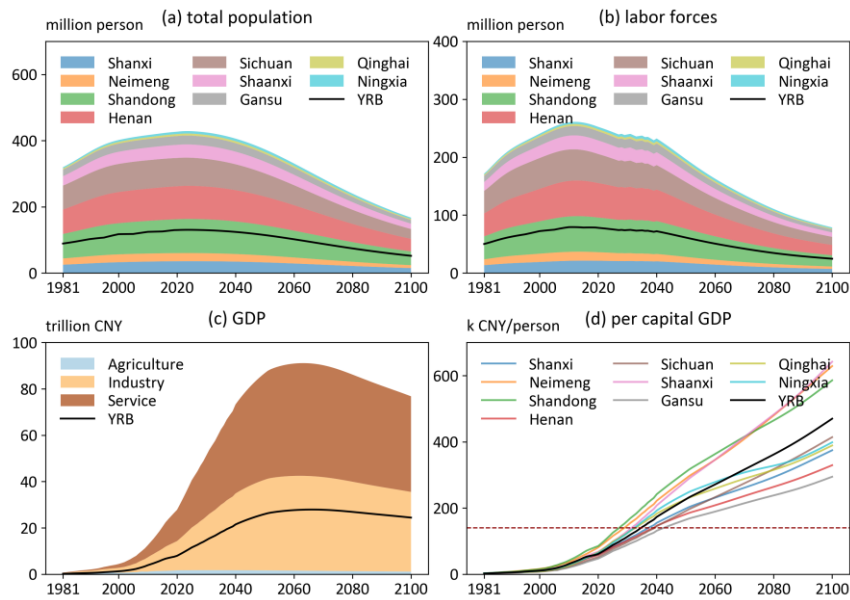
- evapotranspiration
- precipitation
- Precipitation intensity
- CO₂ concentration,

• SSP 2-4.5 — CMIP 6

530 **3.2.2 Projection of CHANS dynamics in future baseline scenario**



531

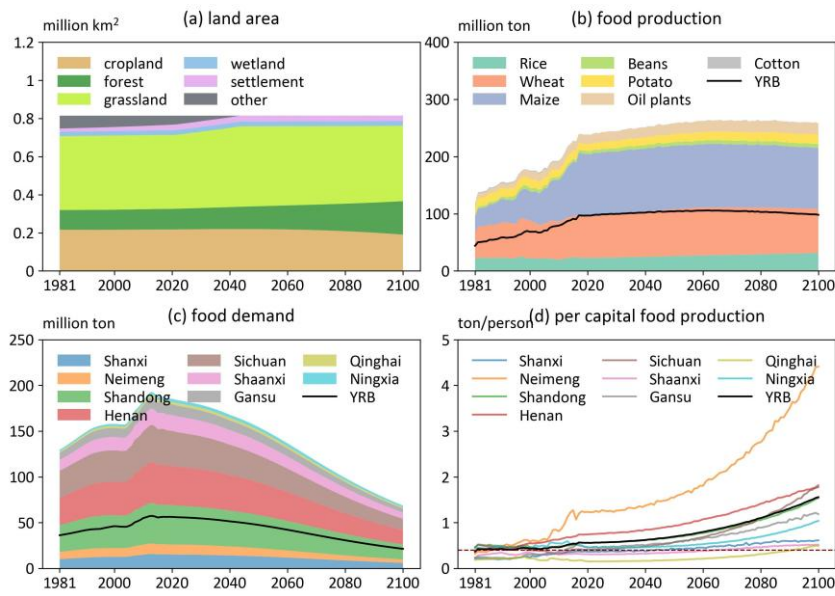


532

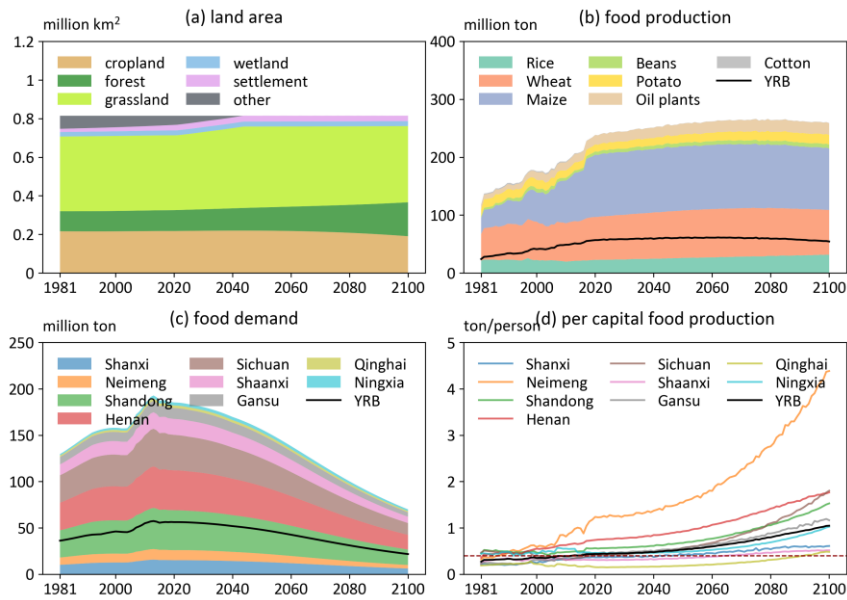
533 Fig.13 Changes in key variables of the *Population* and *Economy* sector in the future
 534 baseline scenario: (a) the total population, (b) the total labor forces, (c) the gross
 535 output of agriculture, industry, and service, and the total gross domestic output, (d) the
 536 per ~~capita~~ capita GDP in nine provinces and YRB.

537 The model simulates human and natural system dynamics under the future
 538 baseline scenario and produces outputs for nine provinces and their corresponding areas
 539 within the YRB. The simulation results are reported either at the provincial level (nine
 540 provinces) for human system sectors or at the basin level (basin boundary) for natural
 541 system sectors. The total population in the nine provinces and the YRB is projected to
 542 peak in 2023 and 2024, at 428429 million and 131 million, respectively, driven by
 543 declining fertility rates. (Fig.13 (a)). The labor force peaks earlier, reaching 249261
 544 million in the nine provinces in 20112012 and 7679 million in the YRB in 20102011
 545 (Fig.13 (b)). After 2025, the labor force is projected to increase again due to the delayed
 546 retirement policy. GDP in the nine provinces is expected to increase until a peak in
 547 20622063, at 7991 trillion CNY (three times the 2020 level, in 2020 constant prices),

548 under the influence of a labor force decline, with the YRB reaching its peak four years
 549 later- (Fig.13 (c)). In contrast to total GDP, per capita GDP in all regions is projected to
 550 continue rising throughout the future period- (Fig.13 (d)). Although all provinces
 551 demonstrate improvements in economic status and living standards, considerable
 552 regional disparities persist. Among the nine provinces, Shaanxi demonstrates the largest
 553 growth in average per capita GDP from 2021 to 2100 relative to the historical period
 554 (1981-2020), with a more than ~~sixteenfold~~~~seventeenfold~~ increase, while the YRB as a
 555 whole shows an over ~~twelvefold~~~~thirteenfold~~ increase.



556

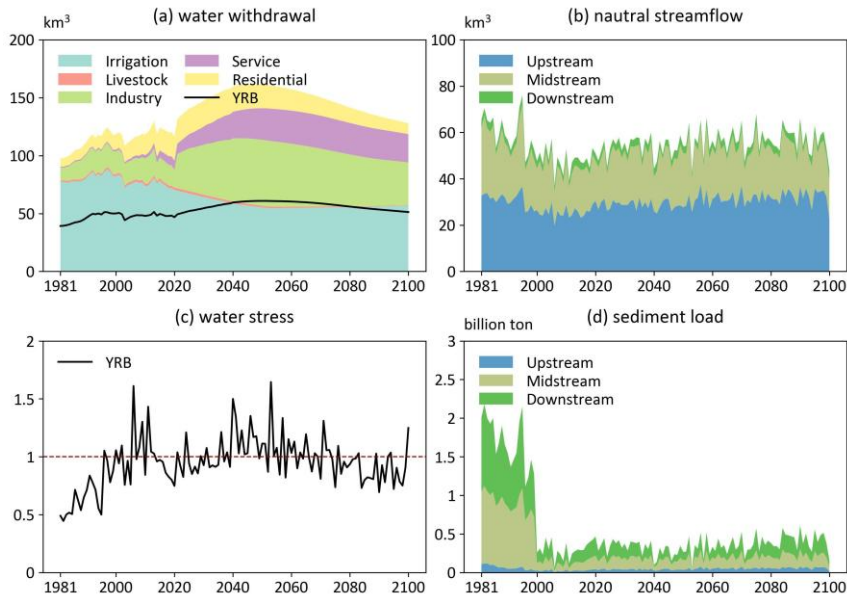


557

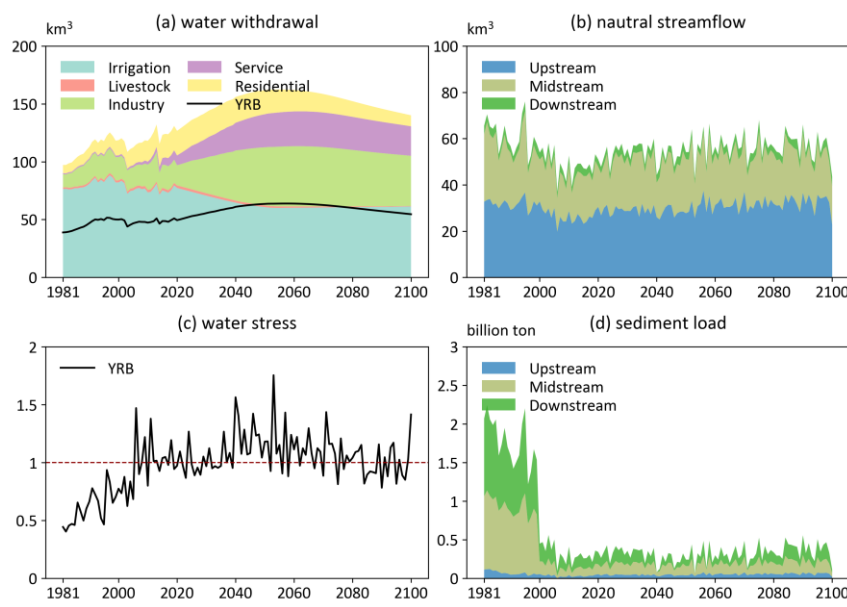
558 Fig.14 Land and food in the future baseline scenario. (a) land area in the YRB; (b-d)
 559 food production of seven crop types, food demand and per ~~capita~~ capita food
 560 production in nine provinces and the YRB, red dotted line represents the 0.4 tons
 561 international food security threshold.

562 Under the future baseline scenario, land use patterns remain relatively stable based
 563 on historical trends, as no new land policies are introduced and cropland area ~~needs~~ has
 564 to stay above the red line- (a mandatory minimum cropland area for each province for
 565 food security) (Fig.14 (a)). The forest area is projected to increase gradually, reaching
 566 62% above the 2021 level by 2100, while the cropland area is expected continue
 567 declining, falling 12% below the 2021 level. Total crop production in nine provinces
 568 and YRB is projected to peak in 2079 and 2062- (Fig.14 (b)), respectively, driven by
 569 the combined effects of declining cropland area and increasing crop yields. Food
 570 demand in both the nine provinces and the YRB as a whole peaked in 2013 (~~192~~193
 571 million tons and 57 million tons, respectively-) (Fig.14 (c)), largely driven by
 572 population dynamics. In the future, per capita food production in the YRB is projected

573 to consistently exceed the international food security threshold of 0.4 tons per person-
 574 (Fig.14 (d)). However, in certain years, provinces such as Qinghai and Shaanxi could
 575 fall below this standard.



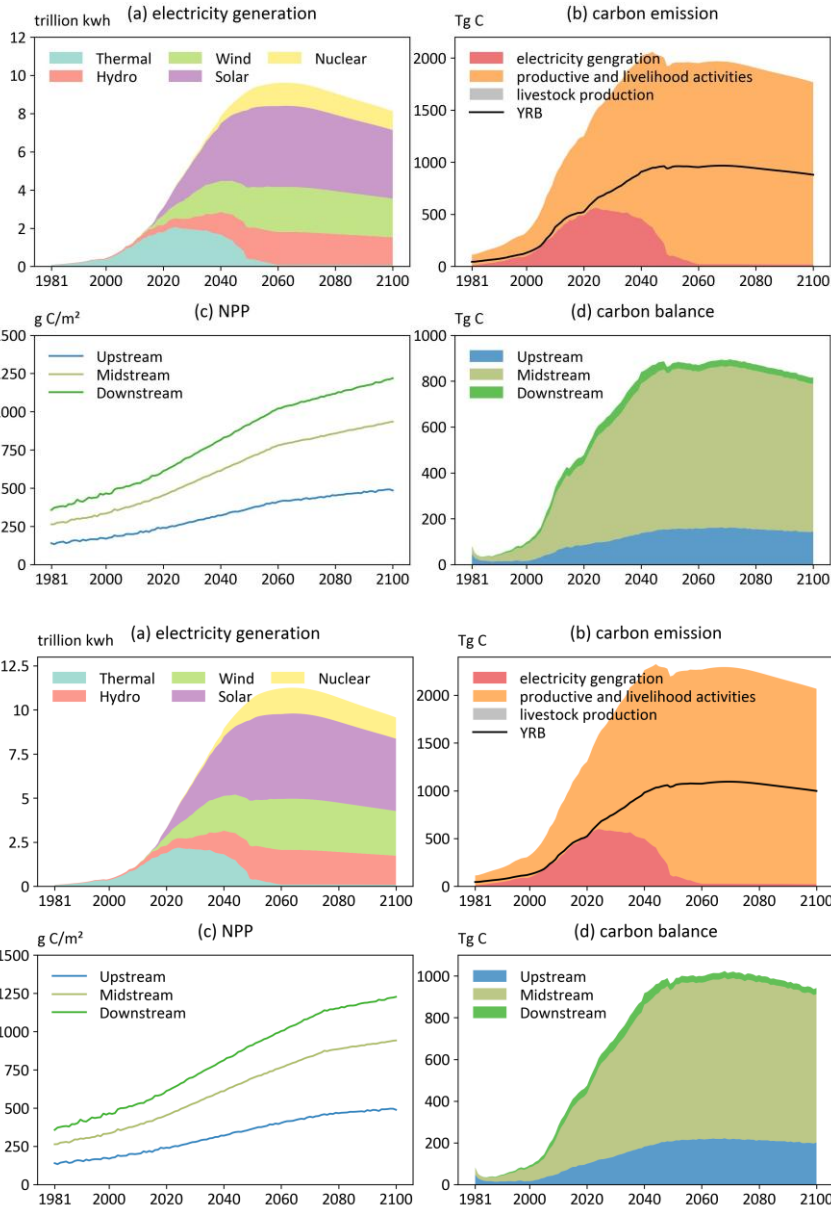
576



577

578 Fig.15 Water demand and supply in the future baseline scenario. (a) water withdrawal
579 across five water-use sectors in nine provinces and the YRB; (b) natural streamflow in
580 up-, mid- and downstream; (c) water stress in the YRB, red dotted line represents the
581 water security threshold; (d) sediment load in the up-, mid- and downstream.

582 Total water withdrawal in the nine provinces and the YRB is projected to peak in
583 ~~2047~~2056 and ~~2051~~2058, reaching 162 km³ and ~~6164~~ km³, respectively. (Fig.15 (a)).
584 Irrigation water withdrawal is expected to decline, driven by reductions in cropland
585 area and irrigation intensity, the latter resulting from improvements in irrigation
586 efficiency assumed in the scenario. Peaks in residential, industrial, service, and
587 livestock water withdrawals are primarily associated with projected peaks in population
588 and GDP. Natural streamflow is projected to ~~follow exhibit~~ a fluctuating upward trend,
589 ~~of 0.073 km³/year basin-wide (Fig. 15(b)), with the future annual mean nearly identical~~
590 ~~to the historical average (a 0.7% increase), and the largest increase occurring most~~
591 ~~significant growth~~ in the upstream region (~~8%~~0.068 km³/year). Considering the
592 ecological flow requirement of 18.7 km³ (YRCCMWR, 2015), water stress (calculated
593 as water consumption divided by (natural discharge - ecological flow)) is expected to
594 decline in the latter half of the century, largely due to the peak and subsequent reduction
595 in water withdrawal. However, overall water stress is projected to exceed historical
596 levels in 2041 and will fall below 1 in ~~5438~~% of the years. (Fig.15 (c)), reflecting
597 ~~mitigation of~~ persistent human-water tensions and future trade-offs between ecological
598 and human water use. As a result of reduced actual streamflow, sediment transport in
599 the Yellow River is projected to decline sharply. (Fig.15 (d)), with a ~~6371~~% decrease in
600 sediment load relative to the historical period.



601

602

603

604

605

Fig.16 Electricity and carbon in the future baseline scenario. (a) the electricity generation from five sources in nine provinces; (b) carbon emission from three sources in nine provinces and the YRB; (c-d) the net primary productivity and carbon

606 balance in the up-, mid-, and downstream.

607 Since the energy system is transitioning to carbon neutrality goals under the future
608 baseline scenario, thermal power generation is projected to decline sharply, while clean
609 energy (hydropower, wind, solar, and nuclear) will become the dominant source for
610 electricity generation- (Fig.16 (a)). The large-scale adoption of clean energy will lead
611 to a peak in carbon emissions from electricity generation in 2024- (Fig.16 (b)). In
612 contrast, emissions from productive and livelihood activities are projected to rise
613 substantially over time, with total human emissions in the YRB reaching a peak in 2044.
614 NPP is anticipated to increase markedly in response to CO₂ concentration increase-
615 (Fig.16 (c)). Although the carbon balance of the YRB has remained positive (net carbon
616 source), it is expected to gradually decline after 2071,2068 (Fig.16 (d)), indicating that
617 the basin's ecosystems alone cannot fully offset human-induced carbon emissions.

618 The above projections of future baseline scenarios highlight persistent challenges
619 to achieving sustainable development in the YRB, underscoring the need for integrated
620 policy responses to address these challenges. Priority should be given to enhancing
621 water-use efficiency and establishing adaptive water resource allocation mechanisms
622 that balance ecological and human water needs. Sediment management strategies,
623 which combine ecological restoration with hydraulic regulation, are necessary to
624 maintain river stability and delta health. To counter the decline in labor force, policies
625 should promote industrial upgrading and technological innovation. Strengthening the
626 basin's carbon mitigation capacity requires accelerating the clean energy transition and
627 expanding ecological restoration to enhance carbon sequestration. Finally, a multi-
628 sectoral, CHANS-based governance framework should be established to coordinate
629 water, land, energy, and carbon management, enabling evidence-based scenario
630 analysis and adaptive policy design for long-term sustainability.

631 **4 Discussion and conclusions**

632 The development of the CHANS-SD-YRB model involves a series of key
633 considerations in translating a conceptual framework into a functioning model. The

634 framework focuses on human–water interactions in the YRB, integrating bidirectional
635 feedback between human and natural processes. SD was chosen to implement the
636 framework, as it effectively captures feedback, non-linear relationships, and cross-
637 sectoral linkages within complex human–natural systems, while remaining practical
638 and straightforward to use. For quantitative representation of human–natural processes,
639 we prefer theoretical methods that incorporate key interactions within the system
640 suitable for implementation using SD. For example, the Budyko framework connects
641 the *Land, Climate, Water Demand, and Water Supply* sectors. Relative to distributed
642 hydrological models, it offers lower computational complexity and reduced data
643 requirements. The Cobb–Douglas production function links the *Population* and
644 *Economy* sectors. Compared with Computable General Equilibrium models (Fujimori
645 et al., 2014a), it is simpler to construct and requires fewer parameters and data inputs.
646 When no suitable theoretical framework/method is available to describe a process, we
647 rely on empirical relationships derived from historical data. For example, crop yields
648 are estimated using fitted relationships between climate variables, fertilizer application,
649 and historical yields. For processes that cannot be represented through empirical
650 functions, we apply literature-based estimates to obtain approximate quantitative
651 relationships, such as fossil fuel emission factors. For processes influenced by external
652 drivers that cannot be endogenously expressed within the model, we quantify them
653 using exogenous parameters derived from historical statistics, such as water intensity.
654 Given the heterogeneous human–natural interactions in the YRB, we represent all
655 processes at the provincial and sub-basin scales using scale-specific parameters, except
656 where parameters or data at these levels are unavailable.

657 The CHANS-SD-YRB model explicitly couples multiple human and natural
658 sectors, enabling a more integrated representation of feedbacks across population,
659 economy, energy, food, water, sediment, land, carbon, and climate. Unlike models that
660 focus on specific sectors or isolated subsystems—such as eco-hydrological models and
661 sediment transport models, which may well capture individual processes but cannot

662 represent the complex human–nature interactions driving system dynamics. Our
663 model’s ~~comprehensive coupling broadens its scope~~integration of application to
664 ~~address complex human and natural sectors~~ provides a robust framework for addressing
665 regional CHANS challenges and ~~provides~~offers practical guidance for sustainable
666 development. The CHANS-SD-YRB model serves as a comprehensive platform for
667 conducting system dynamics prediction, scenario analysis, policy evaluation, and
668 optimization, to alleviate human–water conflicts, ensure food security, and achieve
669 long-term sustainability. For example, analysis of the impacts of the 1987 Yellow River
670 water allocation policy (Song et al., 2024) offer valuable insights for adjusting
671 interprovincial water distribution to promote sustainable water governance; assessment
672 of ecological restoration policies (Li et al., 2015) can guide future ecological
673 engineering; spatiotemporal dynamics of future water gaps can serve as a valuable
674 reference for planning inter-basin water transfers. The model’s flexibility also allows
675 for the incorporation of additional feedback, for example, linking water scarcity to
676 industrial output or climate warming to agricultural productivity. These could include
677 the effects of global warming on human health (Yin et al., 2023a) and economic
678 activities (Nordhaus, 2017), water constraints on production, dietary shifts influencing
679 carbon emissions and land use (Ren et al., 2023), and the trade-offs between carbon
680 mitigation and food security (Xu et al., 2022).

681 Nevertheless, the model remains subject to further refinement. The current
682 simplifications of natural processes could be replaced with more sophisticated models
683 to enhance simulation accuracy. For instance, the YRB hydrological processes involve
684 highly complex human interventions, including reservoir, conservation, and
685 revegetation projects (Wang et al., 2025). The refined runoff simulations by distributed
686 hydrological models improve water supply assessments through their better
687 characterization of spatial heterogeneity in soil, precipitation, and snowmelt (Cong et
688 al., 2009). For human processes, the *Energy* and *Economy* sectors could be refined to
689 model more detailed industry subsectors and emerging trends in energy demand driven

690 by electrification. Moreover, there are still important feedbacks absent from the current
691 coupling framework. Notable examples include the effects of land use change on
692 climate, the effects of climate change on economic growth, and the effects of pricing
693 on energy use and carbon emissions. These missing feedbacks could be incorporated
694 based on recent studies, including the land use feedback on precipitation through
695 moisture recycling (Sang et al., 2025a), socioeconomic losses from impacts of climate
696 change and extremes (Waidelich et al., 2024b), and integration with Computable
697 General Equilibrium (CGE) models (Fujimori et al., 2014b). ~~The~~. Additionally, the
698 model's spatial and temporal resolutions are relatively coarse due to the inherent
699 mismatch in spatiotemporal scales between human and natural processes. The scale at
700 which we make the model represents a practical compromise, constrained by data
701 availability and aligned with the study's objectives. Simulations at finer scales (e.g.,
702 monthly, daily, or gridded) would enhance the representation of natural processes (e.g.,
703 hydrological processes, land use changes, and food production) and the associated
704 spatiotemporal heterogeneity (e.g., daily simulations can assess the impacts of extreme
705 weather). However, it may also exacerbate the scale mismatch with socioeconomic
706 processes, making it challenging to analyze cross-sectoral dynamics. Technically, the
707 inherent limitations of the SD software restrict the model's ability to represent temporal
708 fluctuations and spatial variations. To overcome this, transitioning from the VENSIM
709 platform to a code-based implementation will be necessary, which would also facilitate
710 coupling with other models. Future research should prioritize these improvements to
711 strengthen both the performance and applicability of the model.

712 Overall, the CHANS-SD-YRB ~~Drawing on the conceptual framework of Sang et~~
713 al. (2025), this study implements it into a fully functional, validated System Dynamics
714 model tool, CHANS-SD-YRB 1.0. The model fills the gap in CHANS modeling for the
715 YRB. It integrates the dynamics of ten interconnected sectors: *Population, Economy,*
716 *Energy, Food, Water Demand, Water Supply, Sand, Land, Carbon, and Climate,*
717 achieving reciprocal feedback between human and natural systems. This model can

718 serve as a robust tool to inform policy decisions that influence the evolution of coupled
719 human–natural systems and to explore pathways for optimizing these systems toward
720 sustainability. Furthermore, the modeling process provides valuable experience for
721 regional CHANS modeling and contributes to advancing the broader development of
722 CHANS models at the regional scale.

723 **Code and data availability**

724 The CHANS-SD-YRB V1.0 model (Vensim DSS format), along with the input
725 data and simulation outputs used in this study, are openly accessible at
726 <https://doi.org/10.5281/zenodo.17568963> (Sang, 2025), [and](https://github.com/sangshan-ss/CHANS_SD_YRB)
727 https://github.com/sangshan-ss/CHANS_SD_YRB.

728 **Author contributions**

729 Conceptualization: YL, SS¹, BF. Data curation: SS¹. Formal analysis: SS¹.
730 Funding acquisition: BF, YL. Investigation: YL, SS¹. Methodology: SS¹, YL, BF.
731 Project administration: YL. Resources: YL. Software: SS¹, SZ, LY. Supervision: YL,
732 BF. Validation: SS¹, SZ, LY. Visualization: SS¹. Writing – original draft: SS¹. Writing –
733 review and editing: SS¹, YL, SW, YXL, XTW, SS², WZ, XHW. (Note: SS¹ refers to
734 Shan Sang, and SS² refers to Shuang Song, to distinguish between authors with identical
735 initials.)

736 **Competing interests**

737 The authors declare that they have no conflict of interest.

738 **Acknowledgements**

739 We thank Dr. Weishuang Qu for developing the Threshold 21 model in the
740 Millennium Institute that inspired this study, and also for his and Dr. Haiyan Jiang’s
741 generous help with the CHANS-SD-YRB modeling. We also thank the data support
742 from [Dr. Xianghui Kong, and](#) National Earth System Science Data Center, National
743 Science & Technology Infrastructure of China (<http://www.geodata.cn>).

744 **Financial support**

745 This study is supported by the National Natural Science Foundation of China

746 (Grant No. 42041007), and the Fundamental Research Funds for the Central
747 Universities.

748 **References:**

749 Allen, C., Metternicht, G., Wiedmann, T., and Pedercini, M.: Greater gains for Australia
750 by tackling all SDGs but the last steps will be the most challenging, *Nat Sustain*, 2,
751 1041–1050, <https://doi.org/10.1038/s41893-019-0409-9>, 2019.

752 Breach, P. A. and Simonovic, S. P.: ANEMI3: An updated tool for global change
753 analysis, *PLoS ONE*, 16, e0251489, <https://doi.org/10.1371/journal.pone.0251489>,
754 2021.

755 Calvin, K. and Bond-Lamberty, B.: Integrated human-earth system modeling—state of
756 the science and future directions, *Environ. Res. Lett.*, 13, 063006,
757 <https://doi.org/10.1088/1748-9326/aac642>, 2018.

758 Changming, L. and Shifeng, Z.: Drying up of the yellow river: its impacts and counter-
759 measures, *Mitigation and Adaptation Strategies for Global Change*, 7, 203–214,
760 <https://doi.org/10.1023/A:1024408310869>, 2002.

761 Cheng, Y., Huang, M., Lawrence, D. M., Calvin, K., Lombardozzi, D. L., Sinha, E.,
762 Pan, M., and He, X.: Future bioenergy expansion could alter carbon sequestration
763 potential and exacerbate water stress in the United States, *Science Advances*, 8,
764 eabm8237, <https://doi.org/10.1126/sciadv.abm8237>, 2022.

765 Cobb, C. W. and Douglas, P. H.: A theory of production, *The American Economic*
766 *Review*, 18, 139–165, 1928.

767 Cong, Z., Yang, D., Gao, B., Yang, H., and Hu, H.: Hydrological trend analysis in the
768 Yellow River basin using a distributed hydrological model, *Water Resources Research*,
769 45, 2008WR006852, <https://doi.org/10.1029/2008WR006852>, 2009.

770 Cui, T., Wang, Y., Sun, R., Qiao, C., Fan, W., Jiang, G., Hao, L., and Zhang, L.:
771 Estimating Vegetation Primary Production in the Heihe River Basin of China with
772 Multi-Source and Multi-Scale Data, *PLOS ONE*, 11, e0153971,
773 <https://doi.org/10.1371/journal.pone.0153971>, 2016.

774 Davies, E. G. R. and Simonovic, S. P.: ANEMI: a new model for integrated assessment
775 of global change, *Interdisciplinary Environmental Review*, 2011.

776 Di Vittorio, A. V., Sinha, E., Hao, D., Singh, B., Calvin, K. V., Shippert, T., Patel, P.,
777 and Bond-Lamberty, B.: E3SM-GCAM: A Synchronously Coupled Human Component
778 in the E3SM Earth System Model Enables Novel Human-Earth Feedback Research,
779 *Journal of Advances in Modeling Earth Systems*, 17, e2024MS004806,

780 <https://doi.org/10.1029/2024MS004806>, 2025.

781 Dobbs, G. R., Liu, N., Caldwell, P. V., Miniati, C. F., Sun, G., Duan, K., and Bolstad, P.
782 V.: Inter-basin surface water transfers database for public water supplies in
783 conterminous United States, 1986–2015, *Sci Data*, 10, 255,
784 <https://doi.org/10.1038/s41597-023-02148-5>, 2023.

785 Dottori, F., Szewczyk, W., Ciscar, J.-C., Zhao, F., Alfieri, L., Hirabayashi, Y., Bianchi,
786 A., Mongelli, I., Frieler, K., Betts, R. A., and Feyen, L.: Increased human and economic
787 losses from river flooding with anthropogenic warming, *Nature Clim Change*, 8, 781–
788 786, <https://doi.org/10.1038/s41558-018-0257-z>, 2018.

789 EEA: Trends in atmospheric concentrations of CO₂ (ppm), CH₄ (ppb) and N₂O (ppb),
790 between 1800 and 2017, 2019.

791 Feng, X., Fu, B., Piao, S., Wang, S., Ciais, P., Zeng, Z., Lü, Y., Zeng, Y., Li, Y., Jiang,
792 X., and Wu, B.: Revegetation in China's Loess Plateau is approaching sustainable water
793 resource limits, *Nature Clim Change*, 6, 1019–1022,
794 <https://doi.org/10.1038/nclimate3092>, 2016.

795 Feng, Y. and Zhu, A.: Spatiotemporal differentiation and driving patterns of water
796 utilization intensity in Yellow River Basin of China: Comprehensive perspective on the
797 water quantity and quality, *Journal of Cleaner Production*, 369, 133395,
798 <https://doi.org/10.1016/j.jclepro.2022.133395>, 2022.

799 Flörke, M., Kynast, E., Bärlund, I., Eisner, S., Wimmer, F., and Alcamo, J.: Domestic
800 and industrial water uses of the past 60 years as a mirror of socio-economic
801 development: A global simulation study, *Global Environmental Change*, 23, 144–156,
802 <https://doi.org/10.1016/j.gloenvcha.2012.10.018>, 2013.

803 Forrester, J. W.: *Principles of systems*, Pegasus Communications, Inc, Waltham, MA,
804 1968.

805 Fu, B. and Li, Y.: Bidirectional coupling between the Earth and human systems is
806 essential for modeling sustainability, *National Science Review*, 3, 397–398,
807 <https://doi.org/10.1093/nsr/nww094>, 2016.

808 Fu, B., Liu, Y., Lü, Y., He, C., Zeng, Y., and Wu, B.: Assessing the soil erosion control
809 service of ecosystems change in the Loess Plateau of China, *Ecological Complexity*, 8,
810 284–293, <https://doi.org/10.1016/j.ecocom.2011.07.003>, 2011.

811 Fu, B., Liu, Y., and Meadows, M. E.: Ecological restoration for sustainable
812 development in China, *National Science Review*, 10, nwad033,
813 <https://doi.org/10.1093/nsr/nwad033>, 2023.

814 Fujimori, S., Masui, T., and Matsuoka, Y.: Development of a global computable general
815 equilibrium model coupled with detailed energy end-use technology, *Applied Energy*,
816 128, 296–306, <https://doi.org/10.1016/j.apenergy.2014.04.074>, 2014a.

817 Fujimori, S., Masui, T., and Matsuoka, Y.: Development of a global computable general
818 equilibrium model coupled with detailed energy end-use technology, *Applied Energy*,
819 128, 296–306, <https://doi.org/10.1016/j.apenergy.2014.04.074>, 2014b.

820 Fujimori, S., Wu, W., Doelman, J., Frank, S., Hristov, J., Kyle, P., Sands, R., van Zeist,
821 W.-J., Havlik, P., Domínguez, I. P., Sahoo, A., Stehfest, E., Tabeau, A., Valin, H., van
822 Meijl, H., Hasegawa, T., and Takahashi, K.: Land-based climate change mitigation
823 measures can affect agricultural markets and food security, *Nat Food*, 3, 110–121,
824 <https://doi.org/10.1038/s43016-022-00464-4>, 2022.

825 Gou, J., Miao, C., Samaniego, L., Xiao, M., Wu, J., and Guo, X.: CNRD v1.0: A High-
826 Quality Natural Runoff Dataset for Hydrological and Climate Studies in China, *Bulletin*
827 *of the American Meteorological Society*, 102, E929–E947,
828 <https://doi.org/10.1175/BAMS-D-20-0094.1>, 2021.

829 Hasegawa, T., Sakurai, G., Fujimori, S., Takahashi, K., Hijioka, Y., and Masui, T.:
830 Extreme climate events increase risk of global food insecurity and adaptation needs,
831 *Nat Food*, 2, 587–595, <https://doi.org/10.1038/s43016-021-00335-4>, 2021.

832 Hyun, J.-Y., Huang, S.-Y., Yang, Y.-C. E., Tidwell, V., and Macknick, J.: Using a
833 coupled agent-based modeling approach to analyze the role of risk perception in water
834 management decisions, *Hydrology and Earth System Sciences*, 23, 2261–2278,
835 <https://doi.org/10.5194/hess-23-2261-2019>, 2019.

836 Jain, S., Mindlin, J., Koren, G., Gulizia, C., Steadman, C., Langendijk, G. S., Osman,
837 M., Abid, M. A., Rao, Y., and Rabanal, V.: Are We at Risk of Losing the Current
838 Generation of Climate Researchers to Data Science?, *AGU Advances*, 3,
839 e2022AV000676, <https://doi.org/10.1029/2022AV000676>, 2022.

840 Jia, K., Liang, S., Liu, S., Li, Y., Xiao, Z., Yao, Y., Jiang, B., Zhao, X., Wang, X., Xu,
841 S., and Cui, J.: Global Land Surface Fractional Vegetation Cover Estimation Using
842 General Regression Neural Networks From MODIS Surface Reflectance, *IEEE*
843 *Transactions on Geoscience and Remote Sensing*, 53, 4787–4796,
844 <https://doi.org/10.1109/TGRS.2015.2409563>, 2015.

845 Jia, K., Yang, L., Liang, S., Xiao, Z., Zhao, X., Yao, Y., Zhang, X., Jiang, B., and Liu,
846 D.: Long-Term Global Land Surface Satellite (GLASS) Fractional Vegetation Cover
847 Product Derived From MODIS and AVHRR Data, *IEEE Journal of Selected Topics in*
848 *Applied Earth Observations and Remote Sensing*, 12, 508–518,
849 <https://doi.org/10.1109/JSTARS.2018.2854293>, 2019.

- 850 Jiang, H., Simonovic, S. P., and Yu, Z.: ANEMI_Yangtze v1.0: a coupled human–
851 natural systems model for the Yangtze Economic Belt – model description, *Geosci.*
852 *Model Dev.*, 26, 2022.
- 853 Kemei, Z., Rotich, T., and Bitok, J.: Modelling population dynamics using age-
854 structured system of partial differential equations, *IJAMR*, 13, 110–116,
855 <https://doi.org/10.14419/m81azj37>, 2024.
- 856 Li, M., Shan, R., Abdulla, A., Virguez, E., and Gao, S.: The role of dispatchability in
857 China’s power system decarbonization, *Energy Environ. Sci.*, 17, 2193–2205,
858 <https://doi.org/10.1039/D3EE04293F>, 2024.
- 859 Li, X., Cheng, G., Lin, H., Cai, X., Fang, M., Ge, Y., Hu, X., Chen, M., and Li, W.:
860 Watershed System Model: The Essentials to Model Complex Human-Nature System at
861 the River Basin Scale, *Journal of Geophysical Research: Atmospheres*, 123, 3019–3034,
862 <https://doi.org/10.1002/2017JD028154>, 2018.
- 863 Li, X., Zhang, L., Zheng, Y., Yang, D., Wu, F., Tian, Y., Han, F., Gao, B., Li, H., Zhang,
864 Y., Ge, Y., Cheng, G., Fu, B., Xia, J., Song, C., and Zheng, C.: Novel hybrid coupling
865 of ecohydrology and socioeconomy at river basin scale: A watershed system model for
866 the Heihe River basin, *Environmental Modelling & Software*, 141, 105058,
867 <https://doi.org/10.1016/j.envsoft.2021.105058>, 2021.
- 868 Li, Z., Liu, X., Niu, T., Kejia, D., Zhou, Q., Ma, T., and Gao, Y.: Ecological Restoration
869 and Its Effects on a Regional Climate: The Source Region of the Yellow River, China,
870 *Environ. Sci. Technol.*, 49, 5897–5904, <https://doi.org/10.1021/es505985q>, 2015.
- 871 Liu, C., Golding, D., and Gong, G.: Farmers’ coping response to the low flows in the
872 lower Yellow River: A case study of temporal dimensions of vulnerability, *Global*
873 *Environmental Change*, 18, 543–553, <https://doi.org/10.1016/j.gloenvcha.2008.09.002>,
874 2008.
- 875 Liu, J.: Integration across a metacoupled world, *E&S*, 22, art29,
876 <https://doi.org/10.5751/ES-09830-220429>, 2017.
- 877 Liu, J., Dietz, T., Carpenter, S. R., Alberti, M., Folke, C., Moran, E., Pell, A. N.,
878 Deadman, P., Kratz, T., Lubchenco, J., Ostrom, E., Ouyang, Z., Provencher, W.,
879 Redman, C. L., Schneider, S. H., and Taylor, W. W.: Complexity of Coupled Human
880 and Natural Systems, *Science*, 317, 1513–1516,
881 <https://doi.org/10.1126/science.1144004>, 2007.
- 882 Ministry of Agriculture and Rural Affairs of the People's Republic of China (MAARA),
883 China Agriculture Yearbook,
884 <https://doi.org/https://data.cnki.net/yearBook?type=type&code=A>, 2020.

- 885 Miao, C., Kong, D., Wu, J., and Duan, Q.: Functional degradation of the water–
886 sediment regulation scheme in the lower Yellow River: Spatial and temporal analyses,
887 *Science of The Total Environment*, 551–552, 16–22,
888 <https://doi.org/10.1016/j.scitotenv.2016.02.006>, 2016.
- 889 Miao, C., Gou, J., Fu, B., Tang, Q., Duan, Q., Chen, Z., Lei, H., Chen, J., Guo, J.,
890 Borthwick, A. G. L., Ding, W., Duan, X., Li, Y., Kong, D., Guo, X., and Wu, J.: High-
891 quality reconstruction of China’s natural streamflow, *Science Bulletin*, 67, 547–556,
892 <https://doi.org/10.1016/j.scib.2021.09.022>, 2022.
- 893 Monier, E., Paltsev, S., Sokolov, A., Chen, Y.-H. H., Gao, X., Ejaz, Q., Couzo, E.,
894 Schlosser, C. A., Dutkiewicz, S., Fant, C., Scott, J., Kicklighter, D., Morris, J., Jacoby,
895 H., Prinn, R., and Haigh, M.: Toward a consistent modeling framework to assess multi-
896 sectoral climate impacts, *Nat Commun*, 9, 1–8, [https://doi.org/10.1038/s41467-018-](https://doi.org/10.1038/s41467-018-02984-9)
897 [02984-9](https://doi.org/10.1038/s41467-018-02984-9), 2018.
- 898 Motesharrei, S., Rivas, J., Kalnay, E., Asrar, G. R., Busalacchi, A. J., Cahalan, R. F.,
899 Cane, M. A., Colwell, R. R., Feng, K., Franklin, R. S., Hubacek, K., Miralles-Wilhelm,
900 F., Miyoshi, T., Ruth, M., Sagdeev, R., Shirmohammadi, A., Shukla, J., Srebric, J.,
901 Yakovenko, V. M., and Zeng, N.: Modeling sustainability: population, inequality,
902 consumption, and bidirectional coupling of the Earth and Human Systems, *National*
903 *Science Review*, 3, 470–494, <https://doi.org/10.1093/nsr/nww081>, 2016.
- 904 National Bureau of Statistics of China (NBSC), *China Energy Statistical Yearbook*,
905 <https://doi.org/https://data.cnki.net/yearBook?type=type&code=A>, 2020a.
- 906 National Bureau of Statistics of China (NBSC), *China Population Census Yearbook*,
907 <https://doi.org/https://data.cnki.net/yearBook?type=type&code=A>, 2020b.
- 908 National Bureau of Statistics of China (NBSC), *China Statistical Yearbooks*,
909 <https://doi.org/https://www.stats.gov.cn/english/>, 2020c.
- 910 Ning, X., Zhu, N., Liu, Y., and Wang, H.: Quantifying impacts of climate and human
911 activities on the grassland in the Three-River Headwater Region after two phases of
912 Ecological Project, *Geography and Sustainability*, 3, 164–176,
913 <https://doi.org/10.1016/j.geosus.2022.05.003>, 2022.
- 914 Nordhaus, W. D.: Revisiting the social cost of carbon, *Proceedings of the National*
915 *Academy of Sciences*, 114, 1518–1523, <https://doi.org/10.1073/pnas.1609244114>,
916 2017.
- 917 Qu, W., Shi, W., Zhang, J., and Liu, T.: T21 China 2050: A Tool for National Sustainable
918 Development Planning, *Geography and Sustainability*, 1, 33–46,
919 <https://doi.org/10.1016/j.geosus.2020.03.004>, 2020.

- 920 Rajah, J. K., Blanz, B., Kopainsky, B., and Schoenberg, W.: An endogenous modelling
921 framework of dietary behavioural change in the fully coupled human-climate FRIDA
922 v2.1 model, *Geoscientific Model Development*, 18, 5997–6022,
923 <https://doi.org/10.5194/gmd-18-5997-2025>, 2025.
- 924 Ren, M., Huang, C., Wu, Y., Deppermann, A., Frank, S., Havlik, P., Zhu, Y., Fang, C.,
925 Ma, X., Liu, Y., Zhao, H., Chang, J., Ma, L., Bai, Z., Xu, S., and Dai, H.: Enhanced
926 food system efficiency is the key to China’s 2060 carbon neutrality target, *Nat Food*, 4,
927 552–564, <https://doi.org/10.1038/s43016-023-00790-1>, 2023.
- 928 Richardson, G. P.: Reflections on the foundations of system dynamics, *System
929 Dynamics Review*, 27, 219–243, <https://doi.org/10.1002/sdr.462>, 2011.
- 930 Ristaino, J. B., Anderson, P. K., Bebbler, D. P., Brauman, K. A., Cunniffe, N. J., Fedoroff,
931 N. V., Finegold, C., Garrett, K. A., Gilligan, C. A., Jones, C. M., Martin, M. D.,
932 MacDonald, G. K., Neenan, P., Records, A., Schmale, D. G., Tateosian, L., and Wei, Q.:
933 The persistent threat of emerging plant disease pandemics to global food security,
934 *Proceedings of the National Academy of Sciences*, 118, e2022239118,
935 <https://doi.org/10.1073/pnas.2022239118>, 2021.
- 936 Rydzak, F., Obersteiner, M., Kraxner, F., Fritz, S., and McCallum, I.: FeliX3–Impact
937 Assessment Model: Systemic View across Societal Benefit Areas beyond Global Earth
938 Observation, Laxenburg: International Institute for Applied Systems Analysis (IIASA),
939 2013.
- 940 Sang, S.: CHANS-SD-YRB V1.0: A System Dynamics model of the coupled human-
941 natural systems for the Yellow River Basin (1.0.0),
942 <https://doi.org/https://doi.org/10.5281/zenodo.17568963>, 2025.
- 943 Sang, S., Li, Y., Hou, C., Zi, S., and Lin, H.: The interprovincial green water flow in
944 China and its teleconnected effects on the social economy, *Hydrol. Earth Syst. Sci.*, 29,
945 67–84, <https://doi.org/10.5194/hess-29-67-2025>, 2025a.
- 946 Sang, S., Li, Y., Zong, S., Yu, L., Wang, S., Liu, Y., Wu, X., Song, S., Wang, X., and Fu,
947 B.: The modeling framework of the coupled human and natural systems in the Yellow
948 River Basin, *Geography and Sustainability*, 6, 100294,
949 <https://doi.org/10.1016/j.geosus.2025.100294>, 2025b.
- 950 Shan, Y., Guan, D., Zheng, H., Ou, J., Li, Y., Meng, J., Mi, Z., Liu, Z., and Zhang, Q.:
951 China CO₂ emission accounts 1997–2015, *Sci Data*, 5, 170201,
952 <https://doi.org/10.1038/sdata.2017.201>, 2018.
- 953 Song, S., Wen, H., Wang, S., Wu, X., Cumming, G. S., and Fu, B.: Quantifying the
954 effects of institutional shifts on water governance in the Yellow River Basin: A social-

- 955 ecological system perspective, *Journal of Hydrology*, 629, 130638,
956 <https://doi.org/10.1016/j.jhydrol.2024.130638>, 2024.
- 957 Vaidyanathan, G.: Integrated assessment climate policy models have proven useful,
958 with caveats, *Proc. Natl. Acad. Sci. U.S.A.*, 118, e2101899118,
959 <https://doi.org/10.1073/pnas.2101899118>, 2021.
- 960 Ventana Systems, Inc.: Vensim DSS (version 9.3), 2023.
- 961 Verburg, P. H., Dearing, J. A., Dyke, J. G., Leeuw, S. van der, Seitzinger, S., Steffen,
962 W., and Syvitski, J.: Methods and approaches to modelling the Anthropocene, *Global*
963 *Environmental Change*, 39, 328–340, <https://doi.org/10.1016/j.gloenvcha.2015.08.007>,
964 2016.
- 965 van Vliet, J.: Direct and indirect loss of natural area from urban expansion, *Nat Sustain*,
966 2, 755–763, <https://doi.org/10.1038/s41893-019-0340-0>, 2019.
- 967 Waidelich, P., Batibeniz, F., Rising, J., Kikstra, J. S., and Seneviratne, S. I.: Climate
968 damage projections beyond annual temperature, *Nat. Clim. Chang.*, 14, 592–599,
969 <https://doi.org/10.1038/s41558-024-01990-8>, 2024a.
- 970 Waidelich, P., Batibeniz, F., Rising, J., Kikstra, J. S., and Seneviratne, S. I.: Climate
971 damage projections beyond annual temperature, *Nat. Clim. Chang.*, 14, 592–599,
972 <https://doi.org/10.1038/s41558-024-01990-8>, 2024b.
- 973 Wang, M., Sun, R., Zhu, A., and Xiao, Z.: Evaluation and Comparison of Light Use
974 Efficiency and Gross Primary Productivity Using Three Different Approaches, *Remote*
975 *Sensing*, 12, 1003, <https://doi.org/10.3390/rs12061003>, 2020a.
- 976 Wang, S., Fu, B., Piao, S., Lü, Y., Ciais, P., Feng, X., and Wang, Y.: Reduced sediment
977 transport in the Yellow River due to anthropogenic changes, *Nature Geosci*, 9, 38–41,
978 <https://doi.org/10.1038/ngeo2602>, 2016.
- 979 Wang, S., Song, S., Zhang, H., Yu, L., Jiao, C., Li, C., Wu, X., Zhao, W., Best, J.,
980 Roberts, P., and Fu, B.: Anthropogenic impacts on the Yellow River Basin, *Nat Rev*
981 *Earth Environ*, 6, 656–671, <https://doi.org/10.1038/s43017-025-00718-2>, 2025.
- 982 Wang, T., Teng, F., and Zhang, X.: Assessing global and national economic losses from
983 climate change: a study based on CGEM-IAM in China, *Clim. Change Econ.*, 11,
984 2041003, <https://doi.org/10.1142/S2010007820410031>, 2020b.
- 985 Wang, Y., Zhao, W., Wang, S., Feng, X., and Liu, Y.: Yellow River water rebalanced by
986 human regulation, *Sci Rep*, 9, 9707, <https://doi.org/10.1038/s41598-019-46063-5>, 2019.
- 987 Wei, Z., Jian, Z., Sun, Y., Pan, F., Han, H., Liu, Q., and Mei, Y.: Ecological sustainability

- 988 and high-quality development of the Yellow River Delta in China based on the
989 improved ecological footprint model, *Sci Rep*, 13, 3821,
990 <https://doi.org/10.1038/s41598-023-30896-2>, 2023.
- 991 Wu, J. and Gao, X.: Agridded daily observation dataset over China region and
992 comparison with the other datasets, *Chinese Journal of Geophysics*, 56, 1102–1111,
993 <https://doi.org/10.6038/cjg20130406>, 2013.
- 994 Wu, X., Yan, Z., Yang, H., Wang, S., Zhang, H., Shen, Y., Song, S., Liu, Y., Guo, Y.,
995 Yang, D., and Fu, B.: Ecological restoration in the Yellow River Basin enhances
996 hydropower potential, *Nat Commun*, 16, 2566, <https://doi.org/10.1038/s41467-025-57891-7>, 2025.
- 998 Wu, Z., Li, Y., Wang, R., Xu, X., Ren, D., Huang, Q., Xiong, Y., and Huang, G.:
999 Evaluation of irrigation water saving and salinity control practices of maize and
1000 sunflower in the upper Yellow River basin with an agro-hydrological model based
1001 method, *Agricultural Water Management*, 278, 108157,
1002 <https://doi.org/10.1016/j.agwat.2023.108157>, 2023.
- 1003 Xu, S., Wang, R., Gasser, T., Ciaï, P., Peñuelas, J., Balkanski, Y., Boucher, O., Janssens,
1004 I. A., Sardans, J., Clark, J. H., Cao, J., Xing, X., Chen, J., Wang, L., Tang, X., and Zhang,
1005 R.: Delayed use of bioenergy crops might threaten climate and food security, *Nature*,
1006 609, 299–306, <https://doi.org/10.1038/s41586-022-05055-8>, 2022.
- 1007 Xu, W., Xiao, Y., Zhang, J., Yang, W., Zhang, L., Hull, V., Wang, Z., Zheng, H., Liu, J.,
1008 Polasky, S., Jiang, L., Xiao, Y., Shi, X., Rao, E., Lu, F., Wang, X., Daily, G. C., and
1009 Ouyang, Z.: Strengthening protected areas for biodiversity and ecosystem services in
1010 China, *Proc. Natl. Acad. Sci. U.S.A.*, 114, 1601–1606,
1011 <https://doi.org/10.1073/pnas.1620503114>, 2017.
- 1012 Xu, X., Liu, J., Zhang, S., Li, R., Yan, C., and Wu, S.: China land use remote sensing
1013 monitoring dataset, <https://doi.org/10.12078/2018070201>, 2018.
- 1014 Yan, Z., Wang, T., Ma, T., and Yang, D.: Water-carbon-sediment synergies and trade-
1015 offs: Multi-faceted impacts of large-scale ecological restoration in the Middle Yellow
1016 River Basin, *Journal of Hydrology*, 634, 131099,
1017 <https://doi.org/10.1016/j.jhydrol.2024.131099>, 2024.
- 1018 Yang, D., Shao, W., Yeh, P. J.-F., Yang, H., Kanae, S., and Oki, T.: Impact of vegetation
1019 coverage on regional water balance in the nonhumid regions of China, *Water Resources*
1020 *Research*, 45, <https://doi.org/10.1029/2008WR006948>, 2009.
- 1021 Yang, Z., Li, Q., Xue, W., and Xu, Z.: Impacts of nature reserves on local residents’
1022 income in China, *Ecological Economics*, 199, 107494,

- 1023 <https://doi.org/10.1016/j.ecolecon.2022.107494>, 2022.
- 1024 Ye, Q., Liu, Q., Swamy, D., Gao, L., Moallemi, E. A., Rydzak, F., and Eker, S.: FeliX
1025 2.0: An integrated model of climate, economy, environment, and society interactions,
1026 *Environmental Modelling & Software*, 179, 106121,
1027 <https://doi.org/10.1016/j.envsoft.2024.106121>, 2024.
- 1028 Yin, P., Gao, Y., Chen, R., Liu, W., He, C., Hao, J., Zhou, M., and Kan, H.: Temperature-
1029 related death burden of various neurodegenerative diseases under climate warming: a
1030 nationwide modelling study, *Nat Commun*, 14, 8236, <https://doi.org/10.1038/s41467-023-44066-5>, 2023a.
- 1032 Yin, S., Gao, G., Ran, L., Lu, X., and Fu, B.: Spatiotemporal Variations of Sediment
1033 Discharge and In-Reach Sediment Budget in the Yellow River From the Headwater to
1034 the Delta, *Water Resources Research*, 57, e2021WR030130,
1035 <https://doi.org/10.1029/2021WR030130>, 2021.
- 1036 Yin, S., Gao, G., Ran, L., Li, D., Lu, X., and Fu, B.: Extreme streamflow and sediment
1037 load changes in the Yellow River Basin: Impacts of climate change and human activities,
1038 *Journal of Hydrology*, 619, 129372, <https://doi.org/10.1016/j.jhydrol.2023.129372>,
1039 2023b.
- 1040 Yoon, J., Klassert, C., Selby, P., Lachaut, T., Knox, S., Avisse, N., Harou, J., Tilmant,
1041 A., Klauer, B., Mustafa, D., Sigel, K., Talozzi, S., Gawel, E., Medellín-Azuara, J.,
1042 Bataineh, B., Zhang, H., and Gorelick, S. M.: A coupled human–natural system analysis
1043 of freshwater security under climate and population change, *Proceedings of the*
1044 *National Academy of Sciences*, 118, e2020431118,
1045 <https://doi.org/10.1073/pnas.2020431118>, 2021.
- 1046 Yellow River Conservancy Commission of the Ministry of Water Resources
1047 (YRCCMWR), *Yellow River Basin Comprehensive Planning (2012-2030)*, 2015.
- 1048 Yellow River Conservancy Commission of the Ministry of Water Resources
1049 (YRCCMWR), *Yellow River Water Resources Bulletin*, 2020.
- 1050 Yu, T., Sun, R., Xiao, Z., Zhang, Q., Liu, G., Cui, T., and Wang, J.: Estimation of Global
1051 Vegetation Productivity from Global LAnd Surface Satellite Data, *Remote Sensing*, 10,
1052 327, <https://doi.org/10.3390/rs10020327>, 2018.
- 1053 Zhang, H., Li, R., Cai, X., Zheng, C., Liu, L., Liu, M., Zhang, Q., Lin, H., Chen, L.,
1054 and Wang, X.: Do electricity flows hamper regional economic–environmental equity?,
1055 *Applied Energy*, 326, 120001, <https://doi.org/10.1016/j.apenergy.2022.120001>, 2022a.
- 1056 Zhang, Q., Gu, X., Singh, V. P., Kong, D., and Chen, X.: Spatiotemporal behavior of
1057 floods and droughts and their impacts on agriculture in China, *Global and Planetary*

1058 Change, 131, 63–72, <https://doi.org/10.1016/j.gloplacha.2015.05.007>, 2015.

1059 Zhang, T., Su, X., Zhang, G., Wu, H., and Liu, Y.: Projections of the characteristics and
1060 probability of spatially concurrent hydrological drought in a cascade reservoirs area
1061 under CMIP6, *Journal of Hydrology*, 613, 128472,
1062 <https://doi.org/10.1016/j.jhydrol.2022.128472>, 2022b.

1063 Zhou, F., Bo, Y., Ciais, P., Dumas, P., Tang, Q., Wang, X., Liu, J., Zheng, C., Polcher,
1064 J., Yin, Z., Guimberteau, M., Peng, S., Otle, C., Zhao, X., Zhao, J., Tan, Q., Chen, L.,
1065 Shen, H., Yang, H., Piao, S., Wang, H., and Wada, Y.: Deceleration of China’s human
1066 water use and its key drivers, *Proceedings of the National Academy of Sciences*, 117,
1067 7702–7711, <https://doi.org/10.1073/pnas.1909902117>, 2020.

1068 Zhu, Y., Jia, X., Qiao, J., and Shao, M.: What is the mass of loess in the Loess Plateau
1069 of China?, *Science Bulletin*, 64, 534–539, <https://doi.org/10.1016/j.scib.2019.03.021>,
1070 2019.

1071